SDAC: EFFICIENT SAFE REINFORCEMENT LEARNING WITH LOW-BIASED DISTRIBUTIONAL ACTOR-CRITIC

Anonymous authors
Paper under double-blind review

ABSTRACT

To apply reinforcement learning (RL) to real-world practical applications, agents are required to adhere to the safety guidelines of their respective domains. Safe RL can effectively handle the guidelines by maximizing returns while maintaining safety satisfaction. In this paper, we develop a safe distributional RL method based on the trust region method which has the capability of satisfying safety constraints consistently. However, importance sampling required for the trust region method can hinder performance due to its significant variance, and policies may not meet the safety guidelines due to the estimation bias of distributional critics. Hence, we enhance safety performance through the following approaches. First, we propose novel surrogates for the trust region method expressed with Q-functions using the reparameterization trick. Second, we utilize distributional critics trained with a target distribution where bias-variance can be traded off. In addition, if an initial policy violates safety constraints, there can be no policy satisfying safety constraints within the trust region. Thus, we propose a gradient integration method which is guaranteed to find a policy satisfying multiple constraints from an unsafe initial policy. From extensive experiments, the proposed method shows minimal constraint violations while achieving high returns compared to existing safe RL methods. Furthermore, we demonstrate the benefit of safe RL for problems in which the reward function cannot be easily specified.

1 INTRODUCTION

Deep reinforcement learning (RL) enables reliable control of complex robots at high control frequency (Merel et al., 2020; Peng et al., 2021; Rudin et al., 2022). Miki et al. (2022) have shown that RL can control quadrupedal robots more robustly than existing model-based optimal control methods, and Peng et al. (2022) have performed complex natural motion tasks using physically simulated characters. In order to apply RL to real-world systems, policies should be trained to reflect safety guidelines, which can be realized through reward shaping. The reward shaping process requires designing an additional shaping reward that reflects safety using domain knowledge (Ng et al., 1999), which is a cumbersome and time-consuming task. To avoid these reward shaping tasks, *safe RL* can be an alternative solution, which aims to maximize returns while abiding by user-defined constraints. In a safe RL setting, safety guidelines are represented as constraints of the discounted sum of cost functions that indicate whether the state is safe or not. A cost function is more straightforward to define than a reward function because it only needs a criterion for determining whether a given state is safe. Then, safe policies can be generated using a safe RL algorithm without reward shaping.

There are several constraint types in safe RL. Some constraints focus on the average case using expectation (Achiam et al., 2017; Liu et al., 2022), while others focus on the worst case using risk measures such as conditional value at risk (Yang et al., 2021; Kim & Oh, 2022b). In particular, a distributional critic (Dabney et al., 2018) is required for the worst-case type constraints since their value depends on the shape of the distribution (Zhang & Weng, 2022). There are also various safe RL approaches to find a policy update direction which maximizes returns while satisfying constraints. Among them, plenty of safe RL algorithms (Achiam et al., 2017; Yang et al., 2020; Xu et al., 2021) adopt the trust region method (Schulman et al., 2015) to prevent constraint violation due to a drastic policy change. Moreover, trust region-based methods can guarantee monotonic improvement of the returns while keeping the policy within the feasible region in a tabular setting (Achiam et al., 2017). However, existing methods often suffer from two main issues. First, constraints can be

estimated with large biases if the distributional critics are trained using the one-step distributional Bellmare update (Bellemare et al., 2017), leading to overly conservative or risky policies, as shown in Section 5.3. Second, the trust region method has crucial drawbacks. It uses importance sampling to calculate surrogate functions, which can compromise training stability due to the large variance from the importance sampling. Furthermore, in infeasible starting cases where initial policies do not satisfy constraints, trust region-based methods require a handling method which can project an infeasible policy onto a feasible policy set. However, there is a lack of handling methods when there are multiple constraints.

In this paper, we develop an efficient trust region-based safe RL algorithm with multiple constraints. First, to estimate constraints with low biases, we introduce a *TD(λ) target distribution* combining multiple-step distributions, where bias and variance can be traded off by adjusting the trace-decay λ. Then, under off-policy settings, we present a memory-efficient method to approximate the TD(λ) target distribution using quantile distributions (Dabney et al., 2018), which parameterize a distribution as a sum of Dirac functions. Second, to increase the efficiency of the trust region method, we propose novel surrogate functions which use the reparameterization trick with Q-functions, similar to soft actor-critic (SAC) (Haarnoja et al., 2018), instead of importance sampling. The proposed surrogates can improve training stability due to the absence of the importance ratio and also improve sample efficiency because the policy update direction is directly obtained using Q-functions instead of advantage functions. We empirically show the improvements in Appendix B. Finally, to handle the infeasible starting cases, we propose a gradient integration method, which finds a policy gradient reflecting all constraints, and guarantees to obtain a feasible policy within a finite time under mild technical assumptions. Combining all three approaches, we propose a safe RL method, called a *safe distributional actor-critic* (SDAC).

To evaluate the proposed method, we conduct extensive experiments with four tasks in the Safety Gym environment (Ray et al., 2019) and show that the proposed method achieves high returns with minimal constraint violations during training compared to existing safe RL baselines. Also, we experiment with locomotion tasks using robots with different dynamic models and different numbers of legs to show the advantage of safe RL as it does not require reward shaping. The proposed method has successfully trained locomotion policies with the same straightforward reward and constraints for different robots with different configurations.

2 BACKGROUND

Constrained Markov Decision Processes. We formulate the safe RL problem using constrained Markov decision processes (CMDPs) (Altman, 1999). A CMDP is defined as $(S, A, P, R, C_{1,..,K}, \rho, \gamma)$, where S is a state space, A is an action space, $P : S \times A \times S \mapsto [0, 1]$ is a transition model, $R : S \times A \times S \mapsto \mathbb{R}$ is a reward function, $C_{k\in\{1,...,K\}} : S \times A \times S \mapsto \mathbb{R}_{\geq 0}$ are cost functions, $\rho : S \mapsto [0, 1]$ is an initial state distribution, and $\gamma \in (0, 1)$ is a discount factor. The state action value, state value, and advantage functions are defined as follows:

$$
\begin{aligned}
Q_R^\pi(s,a) &:= \mathop{\mathbb{E}}_{\pi,P}\left[\sum_{t=0}^{\infty}\gamma^t R(s_t,a_t,s_{t+1})\middle| s_0=s, a_0=a\right],\\
V_R^\pi(s) &:= \mathop{\mathbb{E}}_{\pi,P}\left[\sum_{t=0}^{\infty}\gamma^t R(s_t,a_t,s_{t+1})\middle| s_0=s\right], A_R^\pi(s,a) := Q_R^\pi(s,a) - V_R^\pi(s).
\end{aligned}
\tag{1}
$$

By substituting the costs for the reward, the cost value functions $V_{C_k}^\pi(s), Q_{C_k}^\pi(s,a), A_{C_k}^\pi(s,a)$ are defined. In the remainder of the paper, the cost parts will be omitted since they can be retrieved by replacing the reward with the costs. Given a policy π from a stochastic policy set Π, the discounted state distribution is defined as $d^\pi(s) := (1-\gamma)\sum_{t=0}^{\infty}\gamma^t \mathrm{Pr}(s_t = s|\pi)$, and the return is defined as $Z_R^\pi(s,a) := \sum_{t=0}^{\infty}\gamma^t R(s_t,a_t,s_{t+1})$, where $s_0 = s,\ a_0 = a,\ a_t \sim \pi(\cdot|s_t)$, and $s_{t+1} \sim P(\cdot|s_t,a_t)$. Then, the safe RL problem is defined as follows with a safety measure F:

$$
\max_\pi \mathbb{E}\left[Z_R^\pi(s,a)|s\sim\rho, a\sim\pi(\cdot|s)\right] \text{ s.t. } F(Z_{C_k}^\pi(s,a)|s\sim\rho, a\sim\pi(\cdot|s)) \leq d_k\ \forall k, \tag{2}
$$

where d_k is a limit value of the kth constraint.

Mean-Std Constraints. In our safe RL setting, we use mean-std as the safety measure: $F(Z;\alpha) = \mathbb{E}[Z] + (\phi(\Phi^{-1}(\alpha))/\alpha)\cdot\mathrm{Std}[Z]$, where $\alpha \in (0, 1]$ adjusts conservativeness of constraints, $\mathrm{Std}[Z]$ is

the standard deviation of Z, ϕ is the probability density function, and Φ is the cumulative density function of the standard normal distribution. The mean-std is identical to the conditional value at risk (CVaR) if Z follows the Gaussian distribution, and the mean-std constraint can effectively reduce the number of constraint violations, as shown by Yang et al. (2021); Kim & Oh (2022b;a). To estimate the mean-std of cost returns, Kim & Oh (2022b) define the square value functions: $S^{\pi}_{C_k}(s) := \mathop{\mathbb{E}}_{\pi,P}\left[Z^{\pi}_{C_k}(s,a)^2 | a \sim \pi(\cdot|s)\right], S^{\pi}_{C_k}(s,a) := \mathop{\mathbb{E}}_{\pi,P}\left[Z^{\pi}_{C_k}(s,a)^2\right]$, and $A^{\pi}_{S_k}(s,a) := S^{\pi}_{C_k}(s,a) - S^{\pi}_{C_k}(s)$. Additionally, $d^{\pi}_2(s) := (1-\gamma^2)\sum_{t=0}^{\infty}\gamma^{2t}\mathrm{Pr}(s_t = s|\pi)$ denotes a doubly discounted state distribution. Then, the kth constraint can be written as follows:

$$F_k(\pi;\alpha) = J_{C_k}(\pi) + \frac{\phi(\Phi^{-1}(\alpha))}{\alpha}\sqrt{J_{S_k}(\pi) - J_{C_k}(\pi)^2} \leq d_k, \tag{3}$$

where $J_{C_k}(\pi) := \mathop{\mathbb{E}}_{s\sim\rho}\left[V^{\pi}_{C_k}(s)\right]$ and $J_{S_k}(\pi) := \mathop{\mathbb{E}}_{s\sim\rho}\left[S^{\pi}_{C_k}(s)\right]$.

Distributional Quantile Critic. To parameterize the distribution of the returns, Dabney et al. (2018) have proposed an approximation method to estimate the returns using the following quantile distributions, called a *distributional quantile critic*: $\mathrm{Pr}(Z^{\pi}_{R,\theta}(s,a) = z) := \sum_{m=1}^{M}\delta_{\theta_m(s,a)}(z)/M$, where M is the number of atoms, θ is a parametric model, and $\theta_m(s,a)$ is the mth atom. The percentile value of the mth atom is denoted by τ_m ($\tau_0 = 0, \tau_i = i/M$). In distributional RL, the returns are directly estimated to get value functions, and the target distribution can be calculated from the distributional Bellman operator (Bellemare et al., 2017): $\mathcal{T}^{\pi}Z_R(s,a) :\overset{D}{=} R(s,a,s') + \gamma Z_R(s',a')$, where $s' \sim P(\cdot|s,a)$ and $a' \sim \pi(\cdot|s')$. The above one-step operator can be expanded to the n-step one: $\mathcal{T}^{\pi}_n Z_R(s_0,a_0) :\overset{D}{=} \sum_{t=0}^{n-1}\gamma^t R(s_t,a_t,s_{t+1}) + \gamma^n Z_R(s_n,a_n)$. Then, the critic can be trained to minimize the following quantile regression loss (Dabney et al., 2018):

$$\mathcal{L}(\theta) = \sum_{m=1}^{M}\underbrace{\mathbb{E}_{\bar{Z}\sim Z}\left[\rho_{\hat{\tau}_m}(\bar{Z} - \theta_m)\right]}_{=:\mathcal{L}^{\hat{\tau}_m}_{\mathrm{QR}}(\theta_m)}, \text{ where } \rho_{\tau}(x) = x\cdot(\tau - \mathbf{1}_{x<0}),\ \hat{\tau}_m := \frac{\tau_{m-1}+\tau_m}{2}, \tag{4}$$

and $\mathcal{L}^{\tau}_{\mathrm{QR}}(\theta)$ denotes the quantile regression loss for a single atom. The distributional quantile critic can be plugged into existing actor-critic algorithms because only the critic modeling is changed.

3 Proposed Method

We introduce the following three approaches to enhance the safety performance of trust region-based safe RL methods. First, we introduce a TD(λ) target distribution combining n-step distributions, which can trade off bias-variance. The target distribution enables training of the distributional critics with low biases. Second, we propose novel surrogate functions for policy updates that empirically improve the performance of the trust region method. Finally, we present a gradient integration method under multiple constraint settings to handle the infeasible starting cases.

3.1 TD(λ) Target Distribution

We utilize the multiple time-step Bellman operator to reformulate the quantile loss. After collecting trajectories $(s_t, a_t, s_{t+1}, ...)$ with a behavioral policy μ, the n-step targets are estimated as follows,

$$\hat{Z}^{(n)}_t :\overset{D}{=} R_t + \gamma R_{t+1} + \gamma^2 R_{t+2} + \cdots + \gamma^{n-1}R_{t+n-1} + \gamma^n Z^{\pi}_{R,\theta}(s_{t+n}, a'_{t+n}), \tag{5}$$

where $R_t = R(s_t,a_t,s_{t+1})$, $a'_{t+n} \sim \pi(\cdot|s_{t+n})$, and π is the current policy. Note that the n-step target controls the bias-variance tradeoff using n. If n is equal to 1, the n-step target is equivalent to the temporal difference method that has low variance but high bias. On the contrary, if n goes to infinity, it becomes a Monte-Carlo estimation that has high variance but low bias. However, finding proper n is another cumbersome task. To alleviate this issue, TD(λ) (Sutton, 1988) method considers the discounted sum of all n-step targets. Similar to TD(λ), we propose the TD(λ) loss for the distributional quantile critic. The quantile regression loss for a single atom is then approximated

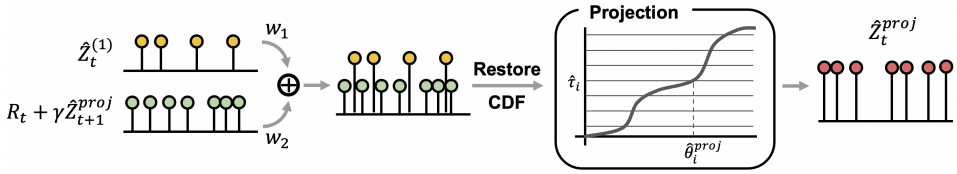

Figure 1: Constructing procedure for target distribution.

as the weighted sum of (4) obtained using the multiple time-step targets and derived as:

$$\begin{aligned}\mathcal{L}_{\mathrm{QR}}^{\tau}(\theta) &= (1-\lambda)\sum_{i=0}^{\infty}\lambda^i \mathbb{E}_{\bar{Z}\sim\mathcal{T}_i^{\pi}Z}\left[\rho_\tau(\bar{Z}-\theta)\right] \\ &\approx \frac{1-\lambda}{M}\sum_{i=0}^{\infty}\lambda^i\prod_{j=1}^{i}\frac{\pi(a_{t+j}|s_{t+j})}{\mu(a_{t+j}|s_{t+j})}\sum_{m=1}^{M}\rho_\tau(\hat{Z}_{t,m}^{(i+1)}-\theta),\end{aligned} \tag{6}$$

where λ is a trace-decay value, and $\hat{Z}_{t,m}^{(i)}$ is the mth atom of $\hat{Z}_t^{(i)}$. Since $\hat{Z}_t^{(i)} \overset{D}{=} R_t + \gamma\hat{Z}_{t+1}^{(i-1)}$ is satisfied, (6) is the same as the quantile regression loss with the following single distribution $\hat{Z}_t^{\mathrm{tot}}$, called a *TD(λ) target distribution*:

$$\begin{aligned}\Pr(\hat{Z}_t^{\mathrm{tot}}=z) &= \frac{1}{\mathcal{N}}\frac{1-\lambda}{M}\sum_{i=0}^{\infty}\lambda^i\prod_{j=1}^{i}\frac{\pi(a_{t+j}|s_{t+j})}{\mu(a_{t+j}|s_{t+j})}\sum_{m=1}^{M}\delta_{\hat{Z}_{t,m}^{(i+1)}}(z) \\ &= \frac{1}{\mathcal{N}}\left\{(1-\lambda)\underbrace{\sum_{m=1}^{M}\frac{1}{M}\delta_{\hat{Z}_{t,m}^{(1)}}(z)}_{\text{One step TD target}} + \lambda\frac{\pi(a_{t+1}|s_{t+1})}{\mu(a_{t+1}|s_{t+1})}\underbrace{\Pr(R_t+\gamma\hat{Z}_{t+1}^{\mathrm{tot}}=z)}_{\text{Previous TD}(\lambda)\text{ target}}\right\},\end{aligned} \tag{7}$$

where $\mathcal{N}$ is a normalization factor. We show that a distribution trained with the proposed target converges to the distribution of Z^π in Appendix A.1. If the target for time step $t+1$ is obtained, the target distribution for time step t becomes the weighted sum distribution of the current one-step TD target and the shifted previous target so that it can be obtained recursively, as shown in (7). However, to obtain the target distribution, we need to store all quantile positions and weights for all time steps, which is not memory-efficient. Therefore, we propose to project the target distribution into a quantile distribution with a specific number of atoms, M' (we set $M' > M$ to reduce information loss). We use Lemma 2 from Dabney et al. (2018) for quantile projection:

$$\hat{\theta}_m = \underset{\theta}{\operatorname{argmin}}\int_{\tau_{m-1}}^{\tau_m}|\mathrm{CDF}^{-1}(w)-\theta|dw = \mathrm{CDF}^{-1}(\hat{\tau}_m),\ \forall m\in\{1,...,M'\}, \tag{8}$$

where CDF is the cumulative distribution function of the original distribution $\hat{Z}_t^{\mathrm{tot}}$, and $\hat{\theta}_m$ is the mth atom of the projected distribution $\hat{Z}_t^{\mathrm{proj}}$. The overall process to get the TD(λ) target distribution is illustrated in Figure 1. After calculating the target distribution for all time steps, the critic can be trained to reduce the quantile regression loss.

3.2 Safe Distributional Actor-Critic

SAC-Style Surrogates. We first extend the surrogate function of the off-policy version of trust region policy optimization (TRPO) (Meng et al., 2022) to include entropy regularization. Then, the entropy-regularized surrogate is modified to be expressed with Q-functions using the reparameterization trick. If we define the objective function with entropy regularization as: $J(\pi) := \mathbb{E}\left[\sum_{t=0}^{\infty}\gamma^t(R(s_t,a_t,s_{t+1})+\beta H(\pi(\cdot|s_t)))|\rho,\pi,P\right]$, where H is the Shannon entropy, the surrogate function (Meng et al., 2022) can be modified as follows:

$$J^{\mu,\pi}(\pi') := \mathbb{E}_{s_0\sim\rho}\left[V^\pi(s_0)\right] + \frac{1}{1-\gamma}\left(\mathop{\mathbb{E}}_{d^\mu,\mu}\left[\frac{\pi'(a|s)}{\mu(a|s)}A^\pi(s,a)\right] + \beta\mathbb{E}_{d^\pi}\left[H(\pi'(\cdot|s))\right]\right), \tag{9}$$

where μ,π,π' are behavioral, current, and next policies, respectively. Then, we can derive a bound on the difference between the objective and surrogate functions.

Theorem 1. *Let us assume that* $\max_s H(\pi(\cdot|s)) < \infty$ *for* $\forall \pi \in \Pi$. *The difference between the objective and surrogate functions is bounded by a term consisting of KL divergence as:*

$$\left|J(\pi') - J^{\mu,\pi}(\pi')\right| \leq \frac{\gamma}{(1-\gamma)^2}\sqrt{D_{\mathrm{KL}}^{\max}(\pi||\pi')}\left(\sqrt{2}\beta\epsilon_H + 2\epsilon_R\sqrt{D_{\mathrm{KL}}^{\max}(\mu||\pi')}\right), \tag{10}$$

where $\epsilon_H = \max_s |H(\pi'(\cdot|s))|$, $\epsilon_R = \max_{s,a} |A^\pi(s,a)|$, $D_{\mathrm{KL}}^{\max}(\pi||\pi') = \max_s D_{\mathrm{KL}}(\pi(\cdot|s)||\pi'(\cdot|s))$, *and the equality holds when* $\pi' = \pi$.

We provide the proof in Appendix A.2. Theorem 1 demonstrates that the surrogate function can approximate the objective function with a small error if the KL divergence is kept small enough. We then introduce a *SAC-style surrogate* by replacing the advantage in (9) with Q-function as follows:

$$\begin{aligned} J^{\mu,\pi}(\pi') &= \mathbb{E}_{s_0\sim\rho}\left[V^\pi(s_0)\right] + \frac{1}{1-\gamma}\left(\mathop{\mathbb{E}}_{d^\mu,\pi'}\left[Q^\pi(s,a)\right] - \mathop{\mathbb{E}}_{d^\mu}\left[V^\pi(s)\right] + \beta\mathbb{E}_{d^\pi}\left[H(\pi'(\cdot|s))\right]\right) \\ &= \frac{1}{1-\gamma}\left(\mathop{\mathbb{E}}_{d^\mu,\pi'}\left[Q^\pi(s,a)\right] + \beta\mathbb{E}_{d^\pi}\left[H(\pi'(\cdot|s))\right]\right) + C, \end{aligned} \tag{11}$$

where C is a constant term for π'. The policy gradient can be calculated using the reparameterization trick, as done in SAC (Haarnoja et al., 2018). We present the training results of the modified off-policy TRPO on continuous RL tasks in Appendix B, where the entropy-regularized (9) and SAC-style (11) versions are compared. Although (9) and (11) are mathematically equivalent, it can be observed that the performance of the SAC-style version is superior to the regularized version. Now, we can apply the same reformulation to the surrogate functions for the safety constraints, which are defined by Kim & Oh (2022a). Hence, the cost surrogate functions $F_k^{\mu,\pi}$ can be written in SAC-style form as follows:

$$\begin{aligned} J_{C_k}^{\mu,\pi}(\pi') &:= \mathbb{E}_{s\sim\rho}\left[V_{C_k}^\pi(s)\right] + \frac{1}{1-\gamma}\mathop{\mathbb{E}}_{d^\mu,\pi'}\left[Q_{C_k}^\pi(s,a)\right] - \frac{1}{1-\gamma}\mathop{\mathbb{E}}_{d^\mu}\left[V_{C_k}^\pi(s)\right], \\ J_{S_k}^{\mu,\pi}(\pi') &:= \mathbb{E}_{s\sim\rho}\left[S_{C_k}^\pi(s)\right] + \frac{1}{1-\gamma^2}\mathop{\mathbb{E}}_{d_2^\mu,\pi'}\left[S_{C_k}^\pi(s,a)\right] - \frac{1}{1-\gamma^2}\mathop{\mathbb{E}}_{d_2^\mu}\left[S_{C_k}^\pi(s)\right], \\ F_k^{\mu,\pi}(\pi';\alpha) &:= J_{C_k}^{\mu,\pi}(\pi') + \frac{\phi(\Phi^{-1}(\alpha))}{\alpha}\sqrt{J_{S_k}^{\mu,\pi}(\pi') - (J_{C_k}^{\mu,\pi}(\pi'))^2}. \end{aligned} \tag{12}$$

Remark that Kim & Oh (2022a) have shown that the cost surrogates are bounded in terms of KL divergence between the current and next policy. Thus, we can construct the following practical, safe policy update rule by adding a trust region constraint:

$$\pi^{\mathrm{new}} = \mathop{\mathrm{argmax}}_{\pi'} J^{\mu,\pi}(\pi') \ \text{ s.t. } F_k^{\mu,\pi}(\pi';\alpha) \leq d_k \ \forall k = 1,...,K, \ D_{\mathrm{KL}}(\pi||\pi') \leq \epsilon, \tag{13}$$

where $D_{\mathrm{KL}}(\pi||\pi') := \mathbb{E}_{s\sim d_\mu}\left[D_{\mathrm{KL}}(\pi(\cdot|s)||\pi'(\cdot|s))\right]$, and ϵ is a trust region size. As (13) is non-linear, the objective and constraints are approximated linearly, while the KL divergence is approximated quadratically in order to determine the update direction. After the direction is obtained, a backtracking line search is performed. For more details, see Appendix A.4.

Approximations. The cost surrogate functions require expectations of the cost value function sampled from the initial distribution, ρ. However, since ρ is not known in the general RL setting, we approximate the surrogate functions by calculating the expectation of the value function sampled from the state distribution of the replay buffer instead of ρ.

$$\begin{aligned} J_C^{\mu,\pi}(\pi') &\approx \frac{1}{1-\gamma}\mathop{\mathbb{E}}_{d^\mu,\pi'}\left[Q_C^\pi(s,a)\right] - \frac{\gamma}{1-\gamma}\mathop{\mathbb{E}}_{d^\mu,\pi}\left[Q_C^\pi(s,a)\right], \\ J_S^{\mu,\pi}(\pi') &\approx \frac{1}{1-\gamma^2}\mathop{\mathbb{E}}_{d_2^\mu,\pi'}\left[S_C^\pi(s,a)\right] - \frac{\gamma^2}{1-\gamma^2}\mathop{\mathbb{E}}_{d_2^\mu,\pi}\left[S_C^\pi(s,a)\right]. \end{aligned} \tag{14}$$

In the distributional RL setting, the cost value and the cost square value functions can be approximated from the quantile distribution as follows:

$$\begin{aligned} Q_C^\pi(s,a) &= \int_{-\infty}^{\infty} z\Pr(Z_C^\pi(s,a) = z)dz \approx \frac{1}{M}\sum_{m=1}^{M}\theta_m(s,a), \\ S_C^\pi(s,a) &= \int_{-\infty}^{\infty} z^2\Pr(Z_C^\pi(s,a) = z)dz \approx \frac{1}{M}\sum_{m=1}^{M}\theta_m(s,a)^2. \end{aligned} \tag{15}$$

Finally, the proposed method is summarized in Algorithm 1.

Algorithm 1: Safe Distributional Actor-Critic

Data: Policy network π_ψ, reward and cost critic networks $Z^\pi_{R,\theta}$, $Z^\pi_{C_k,\theta}$, and replay buffer $\mathcal{D}$.
Initialize network parameters ψ, θ, and replay buffer $\mathcal{D}$.
for *epochs=1, E* **do**
  for *t=1, T* **do**
    Sample $a_t \sim \pi_\psi(\cdot|s_t)$ and get $s_{t+1}, r_t = R(s_t, a_t, s_{t+1}), c_{k,t} = C_k(s_t, a_t, s_{t+1})$.
    Store $(s_t, a_t, \pi_\psi(a_t|s_t), r_t, c_{k,t}, s_{t+1})$ in $\mathcal{D}$.
  end
  Calculate the TD(λ) target distribution (Section 3.1) with $\mathcal{D}$ and update the critics to minimize (4).
  Calculate the surrogate (11) and the cost surrogates using the approximation (14) with $\mathcal{D}$.
  Update the policy by solving (13), but if (13) has no solution, take a recovery step (Section 3.3).
end

3.3 Feasibility Handling For Multiple Constraints

The proposed method updates a policy using (13), but the feasible set of (13) can be empty in the infeasible starting cases. To address the feasibility issue in safe RL with multiple constraints, one of the violated constraints can be selected, and the policy is updated to minimize the constraint until the feasible region is not empty (Xu et al., 2021), which is called a *naive approach*. However, it may not be easy to quickly reach the feasible condition if only one constraint at each update step is used to update the policy. Therefore, we propose a method to reflect all the constraints simultaneously through a gradient integration method used in multi-task learning (Liu et al., 2021; Yu et al., 2020). The main idea is to get a gradient that reduces the value of violated constraints and keeps unviolated constraints. To find such a gradient, the following quadratic program (QP) can be formulated by linearly approximating constraints:

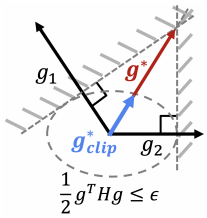

Figure 2: Gradient Integration.

$$g^* = \underset{g}{\operatorname{argmin}} \frac{1}{2} g^T H g \;\; \text{s.t. } g_k^T g + c_k \leq 0, \; \forall k \in \{1, ..., K\}, \tag{16}$$

where H is the Hessian of KL divergence at the current policy parameters ψ, g_k is the gradient of the kth cost surrogate, $c_k = \min(\sqrt{2\epsilon g_k^T H^{-1} g_k}, F_k(\pi_\psi; \alpha) - d_k + \zeta)$, ϵ is a trust region size, and $\zeta \in \mathbb{R}_{>0}$ is a slack coefficient. Finally, we update the policy by $\psi^* = \psi + \min(1, \sqrt{2\epsilon/(g^{*T} H g^*)})g^*$. Figure 2 illustrates the proposed gradient integration process. Each constraint is truncated by c_k to be tangent to the trust region, and the slanted lines show the feasible region of truncated constraints. The solution of (16) is indicated in red, pointing to the nearest point in the intersection of the constraints. If the solution crosses the trust region, parameters are updated by the clipped direction, shown in blue. Then, the policy can reach the feasibility condition within finite time steps.

Theorem 2. *Assume that the cost surrogates are differentiable and convex, gradients of the surrogates are L-Lipschitz continuous, eigenvalues of the Hessian are equal or greater than a positive value $R \in \mathbb{R}_{>0}$, and $\{\psi | F_k(\pi_\psi; \alpha) + \zeta < d_k, \; \forall k\} \neq \emptyset$. Then, there exists $E \in \mathbb{R}_{>0}$ such that if $0 < \epsilon \leq E$ and a policy is updated by the proposed gradient integration method, all constraints are satisfied within finite time steps.*

We provide the proof and show the existence of a solution (16) in Appendix A.3. The provided proof shows that the constant E is proportional to ζ and inversely proportional to the number of constraints K. This means that the trust region size should be set smaller as K increases and ζ decreases. In conclusion, if the policy update rule (13) is not feasible, a finite number of applications of the proposed gradient integration method will make the policy feasible.

4 Related Work

Safe Reinforcement Learning. There are various methods depending on how to update policies to reflect safety constraints. First, trust region-based safe RL methods (Achiam et al., 2017; Yang et al., 2020; Kim & Oh, 2022a) find policy update directions by approximating the safe RL problem

as a linear-quadratic constrained linear program and update policies through a line search. Second, Lagrangian-based methods (Stooke et al., 2020; Yang et al., 2021; Liu et al., 2020) convert the safe RL problem to a dual problem and update the policy and dual variables simultaneously. Last, expectation-maximization (EM) based methods (Liu et al., 2022; Zhang et al., 2022) find non-parametric policy distributions by solving the safe RL problem in E-steps and fit parametric policies to the found non-parametric distributions in M-steps. Also, there are other ways to reflect safety other than policy updates. Qin et al. (2021); Lee et al. (2022) find optimal state or state-action distributions that satisfy constraints, and Bharadhwaj et al. (2021); Thananjeyan et al. (2021) reflect safety during exploration by executing only safe action candidates. In the experiments, only the safe RL methods of the policy update approach are compared with the proposed method.

Distributional TD(λ). TD(λ) (Precup et al., 2000) can be extended to the distributional critic to trade off bias-variance. Gruslys et al. (2018) have proposed a method to obtain target distributions by mixing n-step distributions, but the method is applicable only in discrete action spaces. Nam et al. (2021) have proposed a method to obtain target distributions using sampling to apply to continuous action spaces, but this is only for on-policy settings. A method proposed by Tang et al. (2022) updates the critics using newly defined distributional TD errors rather than target distributions. This method is applicable for off-policy settings but has the disadvantage that memory usage increases linearly with the number of TD error steps. In contrast to these methods, the proposed method is memory-efficient and applicable for continuous action spaces under off-policy settings.

Gradient Integration. The proposed feasibility handling method utilizes a gradient integration method, which is widely used in multi-task learning (MTL). The gradient integration method finds a single gradient to improve all tasks by using gradients of all tasks. Yu et al. (2020) have proposed a projection-based gradient integration method, which is guaranteed to converge Pareto-stationary sets. A method proposed by Liu et al. (2021) can reflect user preference, and Navon et al. (2022) proposed a gradient-scale invariant method to prevent the training process from being biased by a few tasks. The proposed method can be viewed as a mixture of projection and scale-invariant methods as gradients are clipped and projected onto a trust region.

5 Experiments

We evaluate the safety performance of the proposed method and answer whether safe RL actually has the benefit of reducing the effort of reward shaping. For evaluation, agents are trained in the Safety Gym (Ray et al., 2019) with several tasks and robots. To check the advantage of safe RL, we construct locomotion tasks using legged robots with different models and different numbers of legs.

5.1 Safety Gym

Tasks. We employ two robots, point and car, to perform goal and button tasks in the Safety Gym. The goal task is to control a robot toward a randomly spawned goal without passing through hazard regions. The button task is to click a randomly designated button using a robot, where not only hazard regions but also dynamic obstacles exist. Agents get costs when touching undesignated buttons and obstacles or entering hazard regions. Constraint violations (CVs) are counted when a robot contacts obstacles, unassigned buttons, or passes through hazard regions.

Baselines. Safe RL methods based on various types of policy updates are used as baselines. For the trust region-based method, we use constrained policy optimization (CPO) (Achiam et al., 2017) and off-policy trust-region CVaR (OffTRC) (Kim & Oh, 2022a), which extend the CPO to an off-policy and mean-std constrained version. For the Lagrangian-based method, worst-case soft actor-critic (WCSAC) (Yang et al., 2021) is used, and constrained variational policy optimization (CVPO) (Liu et al., 2022) based on the EM method is used. Specifically, WCSAC, OffTRC, and the proposed method, SDAC, use the mean-std constraints, so we experiment with those for $\alpha = 0.25, 0.5$, and 1.0 (when $\alpha = 1.0$, the constraint is identical to the mean constraint).

Results. The graph of the final score and the total number of CVs are shown in Figure 3, and the training curves are provided in Appendix D.1. If points are located in the upper left corner of the graph, the result can be interpreted as excellent since the score is high and the number of CVs is low. The frontiers of SDAC, indicated by the blue dashed lines in Figure 3, are located in the upper left corners for all tasks. Hence, SDAC shows outstanding safety performance compared to other

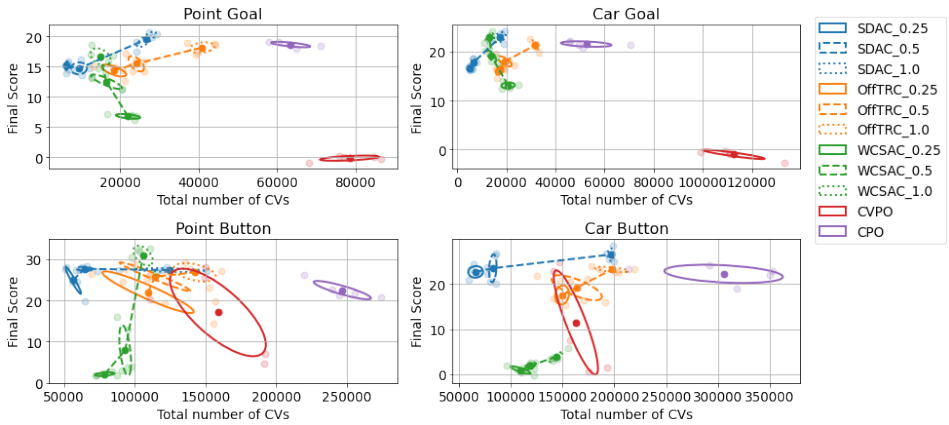

Figure 3: Graphs of final scores and the total number of CVs for the Safety Gym tasks. The number after the algorithm name in the legend indicates α used for the constraint. The center and boundary of ellipses are drawn using the mean and covariance of the five runs for each method. Dashed lines connect results of the same method with different α.

methods. In particular, SDAC with $\alpha = 0.25$ shows comparable scores despite recording the lowest number of CVs in all tasks. Although the frontier overlaps with WCSAC in the car goal and point button tasks, WCSAC shows a high fluctuation of scores depending on the value of α. In addition, it can be seen that the proposed method enhances the efficiency and the training stability of the trust region method since SDAC shows high performance and small covariance compared to the other trust region-based methods, OffTRC and CPO.

5.2 Locomotion Tasks

Tasks. The locomotion tasks are to train robots to follow xy-directional linear and z-directional angular velocity commands. Mini-Cheetah from MIT (Katz et al., 2019) and Laikago from Unitree (Wang, 2018) are used for quadrupedal robots, and Cassie from Agility Robotics (Xie et al., 2018) is used for a bipedal robot. In order to successfully perform the locomotion tasks, robots should keep balancing, standing, and stamping their feet so that they can move in any direction. Therefore, we define three constraints. The first constraint for balancing is to keep the body angle from deviating from zero, and the second for standing is to keep the height of the CoM above a threshold. The final constraint is to match the current foot contact state with a predefined foot contact timing. Especially, the contact timing is defined as stepping off the left and right feet symmetrically. The reward is defined as the negative l^2-norm of the difference between the command and the current velocity. For more details, see Appendix C.

Baselines. Through these tasks, we check the advantage of safe RL over traditional RL. Proximal policy optimization (PPO) (Schulman et al., 2017), based on the trust region method, and truncated quantile critic (TQC) (Kuznetsov et al., 2020), based on the SAC, are used as traditional RL baselines. To apply the same experiment to traditional RL, it is necessary to design a reward reflecting safety. We construct the reward through a weighted sum as $\bar{R} = (R - \sum_{i=1}^{3} w_i C_i)/(1 + \sum_{i=1}^{3} w_i)$, where R and $C_{\{1,2,3\}}$ are used to train safe RL methods and are defined in Appendix C, and R is called the *true reward*. The optimal weights are searched by a Bayesian optimization tool[1], which optimizes the true reward of PPO for the Mini-Cheetah task. The same weights are used for all robots and baselines to verify if reward shaping is required individually for each robot.

Results. Figure 4 shows the true reward sum graphs according to the x-directional velocity command. The overall training curves are presented in Appendix D.2, and the demonstration videos are attached to the supplementary. The figure shows that SDAC performs the locomotion tasks successfully, observing that the reward sums of all tasks are almost zero. PPO shows comparable results in the Mini-Cheetah and Laikago since the reward of the traditional RL baselines is optimized for the Mini-Cheetah task of PPO. However, the reward sum is significantly reduced in the Cassie task, where the kinematic model largely differs from the other robots. TQC shows the lowest reward sums

[1]We use Sweeps from Weights & Biases (Biewald, 2020).

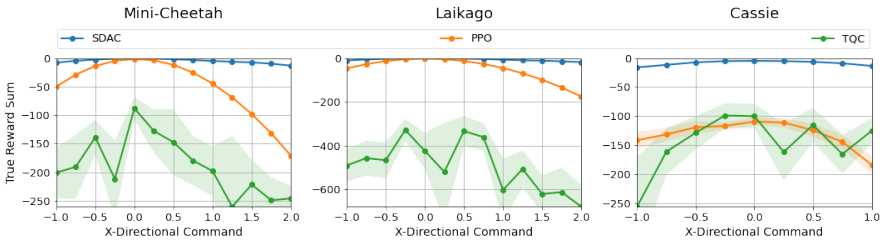

Figure 4: True reward sum graphs according to the x-directional command. The true reward is defined in Appendix C. The solid line and shaded area represent average and one fifth of std value, respectively. The graphs are obtained by running ten episodes per seed for each command.

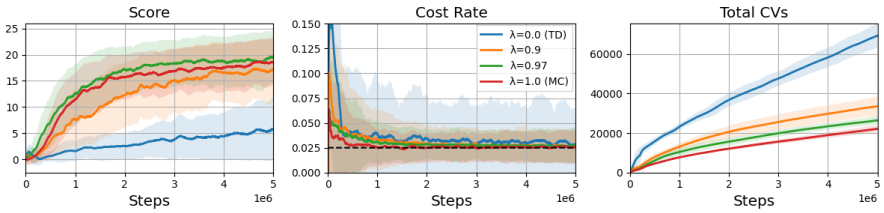

(a) Training curves of the point goal task according to the trace-decay λ.

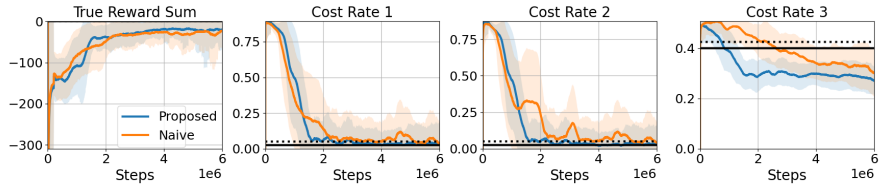

(b) Training curves of the naive and proposed methods for the Cassie task.

Figure 5: Ablation results. The cost rates show the cost sums divided by the episode length. The shaded area represents the standard deviation. The black lines indicate the limit values, and the dotted lines in (b) represent the limit values + 0.025.

despite the state-of-the-art algorithm in other RL benchmarks (Kuznetsov et al., 2020). From these results, it can be observed that reward shaping is required according to algorithms and robots.

5.3 Ablation Study

We conduct ablation studies to show whether the proposed target distribution lowers the estimation bias and whether the proposed gradient integration quickly converges to the feasibility condition. In Figure 5a, the number of CVs is reduced as λ increases, which means that the bias of constraint estimation decreases. However, the score also decreases due to large variance, showing that λ can adjust the bias-variance tradeoff. In Figure 5b, the proposed gradient integration method is compared with a naive approach, which minimizes the constraints in order from the first to the third constraint, as described in Section 3.3. The proposed method reaches the feasibility condition faster than the naive approach and shows stable training curves because it reflects all constraints concurrently.

6 Conclusion

We have presented the trust region-based safe distributional RL method, called *SDAC*. To maximize the merit of the trust region method that can consistently satisfy constraints, we increase the performance by using the Q-function instead of the advantage function in the policy update. We have also proposed the memory-efficient, practical method for finding low-biased target distributions in off-policy settings to estimate constraints. Finally, we proposed the handling method for multiple constraint settings to solve the feasibility issue caused by the trust region method. From extensive the experiments, we have demonstrated that SDAC achieved improved performance with minimal constraint violations and successfully performed the locomotion tasks without reward shaping.

REFERENCES

Joshua Achiam, David Held, Aviv Tamar, and Pieter Abbeel. Constrained policy optimization. In *Proceedings of International Conference on Machine Learning*, pp. 22–31, 2017.

Eitan Altman. *Constrained Markov decision processes*, volume 7. CRC Press, 1999.

Marc G. Bellemare, Will Dabney, and Rémi Munos. A distributional perspective on reinforcement learning. In *Proceedings of International Conference on Machine Learning*, pp. 449–458, 2017.

Marc G. Bellemare, Will Dabney, and Mark Rowland. *Distributional Reinforcement Learning*. MIT Press, 2023. `http://www.distributional-rl.org`.

Homanga Bharadhwaj, Aviral Kumar, Nicholas Rhinehart, Sergey Levine, Florian Shkurti, and Animesh Garg. Conservative safety critics for exploration. In *Proceedings of International Conference on Learning Representations*, 2021.

Lukas Biewald. Experiment tracking with weights and biases, 2020. URL `https://www.wandb.com/`. Software available from wandb.com.

Will Dabney, Mark Rowland, Marc Bellemare, and Rémi Munos. Distributional reinforcement learning with quantile regression. *Proceedings of the AAAI Conference on Artificial Intelligence*, 32(1), 2018.

Audrunas Gruslys, Will Dabney, Mohammad Gheshlaghi Azar, Bilal Piot, Marc Bellemare, and Remi Munos. The reactor: A fast and sample-efficient actor-critic agent for reinforcement learning. In *Proceedings of International Conference on Learning Representations*, 2018.

Tuomas Haarnoja, Aurick Zhou, Pieter Abbeel, and Sergey Levine. Soft actor-critic: Off-policy maximum entropy deep reinforcement learning with a stochastic actor. In *Proceedings of International Conference on Machine Learning*, pp. 1861–1870, 2018.

Benjamin Katz, Jared Di Carlo, and Sangbae Kim. Mini cheetah: A platform for pushing the limits of dynamic quadruped control. In *Proceedings of International Conference on Robotics and Automation*, pp. 6295–6301, 2019.

Dohyeong Kim and Songhwai Oh. Efficient off-policy safe reinforcement learning using trust region conditional value at risk. *IEEE Robotics and Automation Letters*, 7(3):7644–7651, 2022a.

Dohyeong Kim and Songhwai Oh. TRC: Trust region conditional value at risk for safe reinforcement learning. *IEEE Robotics and Automation Letters*, 7(2):2621–2628, 2022b.

Arsenii Kuznetsov, Pavel Shvechikov, Alexander Grishin, and Dmitry Vetrov. Controlling overestimation bias with truncated mixture of continuous distributional quantile critics. In *Proceedings International Conference on Machine Learning*, pp. 5556–5566, 2020.

Jongmin Lee, Cosmin Paduraru, Daniel J Mankowitz, Nicolas Heess, Doina Precup, Kee-Eung Kim, and Arthur Guez. COptiDICE: Offline constrained reinforcement learning via stationary distribution correction estimation. In *Proceedings of International Conference on Learning Representations*, 2022.

Joonho Lee, Jemin Hwangbo, Lorenz Wellhausen, Vladlen Koltun, and Marco Hutter. Learning quadrupedal locomotion over challenging terrain. *Science Robotics*, 5(47):eabc5986, 2020.

Bo Liu, Xingchao Liu, Xiaojie Jin, Peter Stone, and Qiang Liu. Conflict-averse gradient descent for multi-task learning. In *Advances in Neural Information Processing Systems*, pp. 18878–18890, 2021.

Yongshuai Liu, Jiaxin Ding, and Xin Liu. IPO: Interior-point policy optimization under constraints. *Proceedings of the AAAI Conference on Artificial Intelligence*, 34(04):4940–4947, 2020.

Zuxin Liu, Zhepeng Cen, Vladislav Isenbaev, Wei Liu, Steven Wu, Bo Li, and Ding Zhao. Constrained variational policy optimization for safe reinforcement learning. In *Proceedings of International Conference on Machine Learning*, pp. 13644–13668, 2022.

Wenjia Meng, Qian Zheng, Yue Shi, and Gang Pan. An off-policy trust region policy optimization method with monotonic improvement guarantee for deep reinforcement learning. *IEEE Transactions on Neural Networks and Learning Systems*, 33(5):2223–2235, 2022.

Josh Merel, Saran Tunyasuvunakool, Arun Ahuja, Yuval Tassa, Leonard Hasenclever, Vu Pham, Tom Erez, Greg Wayne, and Nicolas Heess. Catch & carry: Reusable neural controllers for vision-guided whole-body tasks. *ACM Transactions on Graphics*, 39(4), 2020.

Takahiro Miki, Joonho Lee, Jemin Hwangbo, Lorenz Wellhausen, Vladlen Koltun, and Marco Hutter. Learning robust perceptive locomotion for quadrupedal robots in the wild. *Science Robotics*, 7(62):eabk2822, 2022.

Daniel W Nam, Younghoon Kim, and Chan Y Park. GMAC: A distributional perspective on actor-critic framework. In *Proceedings of International Conference on Machine Learning*, pp. 7927–7936, 2021.

Aviv Navon, Aviv Shamsian, Idan Achituve, Haggai Maron, Kenji Kawaguchi, Gal Chechik, and Ethan Fetaya. Multi-task learning as a bargaining game. *arXiv preprint arXiv:2202.01017*, 2022.

Andrew Y. Ng, Daishi Harada, and Stuart J. Russell. Policy invariance under reward transformations: Theory and application to reward shaping. In *Proceedings of International Conference on Machine Learning*, pp. 278–287, 1999.

Xue Bin Peng, Ze Ma, Pieter Abbeel, Sergey Levine, and Angjoo Kanazawa. AMP: Adversarial motion priors for stylized physics-based character control. *ACM Transactions on Graphics*, 40 (4), 2021.

Xue Bin Peng, Yunrong Guo, Lina Halper, Sergey Levine, and Sanja Fidler. ASE: Large-scale reusable adversarial skill embeddings for physically simulated characters. *ACM Transactions on Graphics*, 41(4), 2022.

Doina Precup, Richard S. Sutton, and Satinder P. Singh. Eligibility traces for off-policy policy evaluation. In *Proceedings of International Conference on Machine Learning*, pp. 759–766, 2000.

Zengyi Qin, Yuxiao Chen, and Chuchu Fan. Density constrained reinforcement learning. In *Proceedings of International Conference on Machine Learning*, pp. 8682–8692, 2021.

Alex Ray, Joshua Achiam, and Dario Amodei. Benchmarking Safe Exploration in Deep Reinforcement Learning. 2019.

Mark Rowland, Marc Bellemare, Will Dabney, Remi Munos, and Yee Whye Teh. An analysis of categorical distributional reinforcement learning. In *Proceedings of International Conference on Artificial Intelligence and Statistics*, pp. 29–37, 2018.

Nikita Rudin, David Hoeller, Philipp Reist, and Marco Hutter. Learning to walk in minutes using massively parallel deep reinforcement learning. In *Proceedings of Conference on Robot Learning*, pp. 91–100, 2022.

John Schulman, Sergey Levine, Pieter Abbeel, Michael Jordan, and Philipp Moritz. Trust region policy optimization. In *Proceedings of International Conference on Machine Learning*, pp. 1889–1897, 2015.

John Schulman, Filip Wolski, Prafulla Dhariwal, Alec Radford, and Oleg Klimov. Proximal policy optimization algorithms. *arXiv preprint arXiv:1707.06347*, 2017.

Adam Stooke, Joshua Achiam, and Pieter Abbeel. Responsive safety in reinforcement learning by PID lagrangian methods. In *Proceedings of International Conference on Machine Learning*, pp. 9133–9143, 2020.

Richard S Sutton. Learning to predict by the methods of temporal differences. *Machine learning*, 3 (1):9–44, 1988.

Yunhao Tang, Mark Rowland, Rémi Munos, Bernardo Ávila Pires, Will Dabney, and Marc G Bellemare. The nature of temporal difference errors in multi-step distributional reinforcement learning. *arXiv preprint arXiv:2207.07570*, 2022.

Brijen Thananjeyan, Ashwin Balakrishna, Suraj Nair, Michael Luo, Krishnan Srinivasan, Minho Hwang, Joseph E. Gonzalez, Julian Ibarz, Chelsea Finn, and Ken Goldberg. Recovery RL: Safe reinforcement learning with learned recovery zones. *IEEE Robotics and Automation Letters*, 6 (3):4915–4922, 2021.

Emanuel Todorov, Tom Erez, and Yuval Tassa. MuJoCo: A physics engine for model-based control. In *Proceedings of International Conference on Intelligent Robots and Systems*, pp. 5026–5033, 2012.

Xingxing Wang. Unitree-Laikago Pro. `http://www.unitree.cc/e/action/ShowInfo.php?classid=6&id=355`, 2018.

Zhaoming Xie, Glen Berseth, Patrick Clary, Jonathan Hurst, and Michiel van de Panne. Feedback control for cassie with deep reinforcement learning. In *Proceedings of International Conference on Intelligent Robots and Systems*, pp. 1241–1246, 2018.

Tengyu Xu, Yingbin Liang, and Guanghui Lan. CRPO: A new approach for safe reinforcement learning with convergence guarantee. In *Proceedings of International Conference on Machine Learning*, pp. 11480–11491, 2021.

Qisong Yang, Thiago D. Simão, Simon H Tindemans, and Matthijs T. J. Spaan. WCSAC: Worst-case soft actor critic for safety-constrained reinforcement learning. *Proceedings of the AAAI Conference on Artificial Intelligence*, 35(12):10639–10646, 2021.

Tsung-Yen Yang, Justinian Rosca, Karthik Narasimhan, and Peter J. Ramadge. Projection-based constrained policy optimization. In *Proceedings of International Conference on Learning Representations*, 2020.

Tianhe Yu, Saurabh Kumar, Abhishek Gupta, Sergey Levine, Karol Hausman, and Chelsea Finn. Gradient surgery for multi-task learning. In *Advances in Neural Information Processing Systems*, pp. 5824–5836, 2020.

Hengrui Zhang, Youfang Lin, Sheng Han, Shuo Wang, and Kai Lv. Conservative distributional reinforcement learning with safety constraints. *arXiv preprint arXiv:2201.07286*, 2022.

Jianyi Zhang and Paul Weng. Safe distributional reinforcement learning. In Jie Chen, Jérôme Lang, Christopher Amato, and Dengji Zhao (eds.), *Proceedings of International Conference on Distributed Artificial Intelligence*, pp. 107–128, 2022.

A Algorithm Details

A.1 Convergence Analysis

In this section, we show that the proposed TD(λ) target distribution converges to the Z^π. First, we express the target distribution using a distributional operator and show that the operator is contractive. Finally, we show that Z^π is the unique fixed point.

Before starting the proof, we introduce useful notions, distance metrics, and operators. As the return $Z^\pi(s,a)$ is a random variable, we define the distribution of $Z^\pi(s,a)$ as $\nu^\pi(s,a)$. Let η be the distribution of a random variable X. Then, we can express the distribution of affine transformation of random variable, $aX+b$, using the *pushforward* operator, which is defined by Rowland et al. (2018), as $(f_{a,b})_\#(\eta)$. To measure a distance between two distributions, Bellemare et al. (2023) has defined the distance l_p as follows:

$$l_p(\eta_1,\eta_2) := \left(\int_{\mathbb{R}} |F_{\eta_1}(x) - F_{\eta_2}(x)|^p \, dx\right)^{1/p}, \tag{17}$$

where $F_\nu(z)$ is the cumulative distribution function. This distance is $1/p$-homogeneous, regular, and p-convex (see Section 4 of Bellemare et al. (2023) for more details). For functions that map state-action pairs to distributions, a distance can be defined as (Bellemare et al., 2023): $\bar{l}_p(\nu_1,\nu_2) := \sup_{(s,a)\in S\times A} l_p(\nu_1(s,a),\nu_2(s,a))$. Then, the proposed TD($\lambda$) target distribution can be expressed as an operator as below.

$$\begin{aligned}\mathcal{T}_\lambda^{\mu,\pi}\nu(s,a) &:= \frac{1-\lambda}{\mathcal{N}}\sum_{i=0}^{\infty}\lambda^i \\ &\times \mathbb{E}_\mu\left[\left(\prod_{j=1}^{i}\eta(s_j,a_j)\right)\mathbb{E}_{a'\sim\pi(\cdot|s_{i+1})}\left[(f_{\gamma^{i+1},\sum_{t=0}^{i}\gamma^t r_t})_\#(\nu(s_{i+1},a'))\right]\Big| s_0=s, a_0=a\right],\end{aligned} \tag{18}$$

where $\eta(s,a) = \frac{\pi(a|s)}{\mu(a|s)}$. Then, the operator $\mathcal{T}_\lambda^{\mu,\pi}$ has a contraction property.

Theorem 3. *Under the distance $\bar{l}_p$ and the assumption that the state, action, and reward spaces are finite, $\mathcal{T}_\lambda^{\mu,\pi}$ is $\gamma^{1/p}$-contractive.*

Proof. First, the operator can be rewritten using summation as follows.

$$\begin{aligned}\mathcal{T}_\lambda^{\mu,\pi}\nu(s,a) &= \frac{1-\lambda}{\mathcal{N}}\sum_{i=0}^{\infty}\lambda^i\sum_{a'\in A}\sum_{(s_0,a_0,r_0,\ldots,s_{i+1})}\Pr_\mu(\underbrace{s_0,a_0,r_0,\ldots,s_{i+1}}_{=:\tau})\left(\prod_{j=1}^{i}\eta(s_j,a_j)\right) \\ &\quad\times\pi(a'|s_{i+1})(f_{\gamma^{i+1},\sum_{t=0}^{i}\gamma^t r_t})_\#(\nu(s_{i+1},a')) \\ &= \frac{1-\lambda}{\mathcal{N}}\sum_{i=0}^{\infty}\lambda^i\sum_{a'\in A}\sum_{\tau}\Pr_\mu(\tau)\left(\prod_{j=1}^{i}\eta(s_j,a_j)\right)\pi(a'|s_{i+1})\sum_{s'\in S}\mathbf{1}_{s'=s_{i+1}} \\ &\quad\times\sum_{r'_{0:i}}\left(\prod_{k=0}^{i}\mathbf{1}_{r'_k=r_k}\right)(f_{\gamma^{i+1},\sum_{t=0}^{i}\gamma^t r'_t})_\#(\nu(s',a')) \\ &= \frac{1-\lambda}{\mathcal{N}}\sum_{i=0}^{\infty}\lambda^i\sum_{a'\in A}\sum_{s'\in S}\sum_{r'_{0:i}}(f_{\gamma^{i+1},\sum_{t=0}^{i}\gamma^t r'_t})_\#(\nu(s',a')) \\ &\quad\times\underbrace{\mathbb{E}_\mu\left[\left(\prod_{j=1}^{i}\eta(s_j,a_j)\right)\pi(a'|s_{i+1})\mathbf{1}_{s'=s_{i+1}}\left(\prod_{k=0}^{i}\mathbf{1}_{r'_k=r_k}\right)\right]}_{=:w_{s',a',r'_{0:i}}} \\ &= \frac{1-\lambda}{\mathcal{N}}\sum_{i=0}^{\infty}\sum_{s'\in S}\sum_{a'\in A}\sum_{r'_{0:i}}\lambda^i w_{s',a',r'_{0:i}}(f_{\gamma^{i+1},\sum_{t=0}^{i}\gamma^t r'_t})_\#(\nu(s',a')).\end{aligned} \tag{19}$$

Since the sum of weights of distributions should be one, we can find the normalization factor $\mathcal{N} = (1-\lambda)\sum_{i=0}^{\infty}\sum_{s\in S}\sum_{a\in A}\sum_{r_{0:i}}\lambda^i w_{s,a,r_{0:i}}$. Then, the following inequality can be derived using the homogeneity, regularity, and convexity of l_p:

$$
\begin{aligned}
& l_p^p(\mathcal{T}_\lambda^{\mu,\pi}\nu_1(s,a), \mathcal{T}_\lambda^{\mu,\pi}\nu_2(s,a)) \\
&= l_p^p\Bigg(\frac{1-\lambda}{\mathcal{N}}\sum_{i=0}^{\infty}\sum_{s\in S}\sum_{a\in A}\sum_{r_{0:i}}\lambda^i w_{s,a,r_{0:i}}(f_{\gamma^{i+1},\sum_{t=0}^{i}\gamma^t r_t})_\#(\nu_1(s,a)), \\
&\qquad \frac{1-\lambda}{\mathcal{N}}\sum_{i=0}^{\infty}\sum_{s\in S}\sum_{a\in A}\sum_{r_{0:i}}\lambda^i w_{s,a,r_{0:i}}(f_{\gamma^{i+1},\sum_{t=0}^{i}\gamma^t r_t})_\#(\nu_2(s,a))\Bigg) \\
&\le \sum_{i=0}^{\infty}\sum_{s\in S}\sum_{a\in A}\sum_{r_{0:i}}\frac{(1-\lambda)\lambda^i w_{s,a,r_{0:i}}}{\mathcal{N}} l_p^p\Big((f_{\gamma^{i+1},\sum_{t=0}^{i}\gamma^t r_t})_\#(\nu_1(s,a)), \\
&\qquad (f_{\gamma^{i+1},\sum_{t=0}^{i}\gamma^t r_t})_\#(\nu_2(s,a))\Big) \\
&\le \sum_{i=0}^{\infty}\sum_{s\in S}\sum_{a\in A}\sum_{r_{0:i}}\frac{(1-\lambda)\lambda^i w_{s,a,r_{0:i}}}{\mathcal{N}} l_p^p\left((f_{\gamma^{i+1},0})_\#(\nu_1(s,a)), (f_{\gamma^{i+1},0})_\#(\nu_2(s,a))\right) \\
&= \sum_{i=0}^{\infty}\sum_{s\in S}\sum_{a\in A}\sum_{r_{0:i}}\frac{(1-\lambda)\lambda^i w_{s,a,r_{0:i}}}{\mathcal{N}}\gamma^{i+1} l_p^p\left(\nu_1(s,a), \nu_2(s,a)\right) \\
&\le \sum_{i=0}^{\infty}\sum_{s\in S}\sum_{a\in A}\sum_{r_{0:i}}\frac{(1-\lambda)\lambda^i w_{s,a,r_{0:i}}}{\mathcal{N}}\gamma^{i+1}\left(\bar{l}_p\left(\nu_1,\nu_2\right)\right)^p \\
&\le \gamma\left(\bar{l}_p\left(\nu_1,\nu_2\right)\right)^p.
\end{aligned} \tag{20}
$$

Therefore, $\bar{l}_p\left(\mathcal{T}_\lambda^{\mu,\pi}\nu_1, \mathcal{T}_\lambda^{\mu,\pi}\nu_2\right) \le \gamma^{1/p}\bar{l}_p\left(\nu_1,\nu_2\right)$. □

By the Banach's fixed point theorem, the operator has a unique fixed distribution. From the definition of Z^π, the following equality holds (Rowland et al., 2018): $\nu^\pi(s,a) = \mathbb{E}_\pi\left[(f_{\gamma,r})_\#(\nu^\pi(s',a'))\right]$. Then, it can be shown that ν^π is the fixed distribution by applying the operator $\mathcal{T}_\lambda^{\mu,\pi}$ to ν^π:

$$
\begin{aligned}
& \mathcal{T}_\lambda^{\mu,\pi}\nu^\pi(s,a) = \frac{1-\lambda}{\mathcal{N}}\sum_{i=0}^{\infty}\lambda^i \\
& \times \mathbb{E}_\mu\left[\left(\prod_{j=1}^{i}\eta(s_j,a_j)\right)\mathbb{E}_{a'\sim\pi(\cdot|s_{i+1})}\left[(f_{\gamma^{i+1},\sum_{t=0}^{i}\gamma^t r_t})_\#(\nu^\pi(s_{i+1},a'))\right]\Big| s_0=s, a_0=a\right] \\
&= \frac{1-\lambda}{\mathcal{N}}\sum_{i=0}^{\infty}\lambda^i\mathbb{E}_\pi\left[(f_{\gamma^{i+1},\sum_{t=0}^{i}\gamma^t r_t})_\#(\nu^\pi(s_{i+1},a_{i+1}))\Big| s_0=s, a_0=a\right] \\
&= \frac{1-\lambda}{\mathcal{N}}\sum_{i=0}^{\infty}\lambda^i\nu^\pi(s,a) = \nu^\pi(s,a).
\end{aligned} \tag{21}
$$

A.2 Proof of Theorem 1

Before showing the proof, we present a new function and a lemma. A value difference function is defined as follows:

$$
\delta^{\pi'}(s) := \mathbb{E}\left[R(s,a,s') + \gamma V^\pi(s') - V^\pi(s) \mid a\sim\pi'(\cdot|s), s'\sim P(\cdot|s,a)\right] = \mathop{\mathbb{E}}_{a\sim\pi'}\left[A^\pi(s,a)\right].
$$

Lemma 4. *The maximum of $|\delta^{\pi'}(s) - \delta^\pi(s)|$ is equal or less than $\epsilon_R\sqrt{2D_{\mathrm{KL}}^{\max}(\pi||\pi')}$.*

Proof. The value difference can be expressed in a vector form,

$$
\delta^{\pi'}(s) - \delta^\pi(s) = \sum_a(\pi'(a|s) - \pi(a|s))A^\pi(s,a) = \langle\pi'(\cdot|s) - \pi(\cdot|s), A^\pi(s,\cdot)\rangle.
$$

Using Hölder's inequality, the following inequality holds:

$$\begin{aligned}|\delta^{\pi'}(s) - \delta^{\pi}(s)| &\leq ||\pi'(\cdot|s) - \pi(\cdot|s)||_1 \cdot ||A^{\pi}(s,\cdot)||_\infty \\ &= 2D_{\mathrm{TV}}(\pi'(\cdot|s)||\pi(\cdot|s))\max_a A^{\pi}(s,a).\end{aligned}$$

$$\Rightarrow ||\delta^{\pi'} - \delta^{\pi}||_\infty = \max_s |\delta^{\pi'}(s) - \delta^{\pi}(s)| \leq 2\epsilon_R \max_s D_{\mathrm{TV}}(\pi(\cdot|s)||\pi'(\cdot|s)).$$

Using Pinsker's inequality, $||\delta^{\pi'} - \delta^{\pi}||_\infty \leq \epsilon_R\sqrt{2D_{\mathrm{KL}}^{\max}(\pi||\pi')}$. □

Theorem 1. *Let us assume that* $\max_s H(\pi(\cdot|s)) < \infty$ *for* $\forall\pi \in \Pi$. *The difference between the objective and surrogate functions is bounded by a term consisting of KL divergence as:*

$$\left|J(\pi') - J^{\mu,\pi}(\pi')\right| \leq \frac{\gamma}{(1-\gamma)^2}\sqrt{D_{\mathrm{KL}}^{\max}(\pi||\pi')}\left(\sqrt{2}\beta\epsilon_H + 2\epsilon_R\sqrt{D_{\mathrm{KL}}^{\max}(\mu||\pi')}\right), \tag{10}$$

where $\epsilon_H = \max_s |H(\pi'(\cdot|s))|$, $\epsilon_R = \max_{s,a} |A^{\pi}(s,a)|$, $D_{\mathrm{KL}}^{\max}(\pi||\pi') = \max_s D_{\mathrm{KL}}(\pi(\cdot|s)||\pi'(\cdot|s))$, *and the equality holds when* $\pi' = \pi$.

Proof. The surrogate function can be expressed in vector form as follows:

$$J^{\mu,\pi}(\pi') = \langle\rho, V^{\pi}\rangle + \frac{1}{1-\gamma}\left(\langle d^{\mu}, \delta^{\pi'}\rangle + \beta\langle d^{\pi}, H^{\pi'}\rangle\right),$$

where $H^{\pi'}(s) = H(\pi'(\cdot|s))$. The objective function of π' can also be expressed in a vector form using Lemma 1 from Achiam et al. (2017),

$$\begin{aligned}J(\pi') &= \frac{1}{1-\gamma}\mathbb{E}\left[R(s,a,s') + \beta H^{\pi'}(s) \mid s \sim d^{\pi'}, a \sim \pi'(\cdot|s), s' \sim P(\cdot|s,a)\right] \\ &= \frac{1}{1-\gamma}\mathop{\mathbb{E}}_{s\sim d^{\pi'}}\left[\delta^{\pi'}(s) + \beta H^{\pi'}(s)\right] + \mathop{\mathbb{E}}_{s\sim\rho}\left[V^{\pi}(s)\right] \\ &= \langle\rho, V^{\pi}\rangle + \frac{1}{1-\gamma}\langle d^{\pi'}, \delta^{\pi'} + \beta H^{\pi'}\rangle.\end{aligned}$$

By Lemma 3 from Achiam et al. (2017), $||d^{\pi} - d^{\pi'}||_1 \leq \frac{\gamma}{1-\gamma}\sqrt{2D_{\mathrm{KL}}^{\max}(\pi||\pi')}$. Then, the following inequality is satisfied:

$$\begin{aligned}&|(1-\gamma)(J^{\mu,\pi}(\pi') - J(\pi'))| \\ &\quad= |\langle d^{\pi'} - d^{\mu}, \delta^{\pi'}\rangle + \beta\langle d^{\pi} - d^{\pi'}, H^{\pi'}\rangle| \\ &\quad\leq |\langle d^{\pi'} - d^{\mu}, \delta^{\pi'}\rangle| + \beta|\langle d^{\pi} - d^{\pi'}, H^{\pi'}\rangle| \\ &\quad= |\langle d^{\pi'} - d^{\mu}, \delta^{\pi'} - \delta^{\pi}\rangle| + \beta|\langle d^{\pi} - d^{\pi'}, H^{\pi'}\rangle| && (\because \delta^{\pi} = 0) \\ &\quad\leq ||d^{\pi'} - d^{\mu}||_1||\delta^{\pi'} - \delta^{\pi}||_\infty + \beta||d^{\pi} - d^{\pi'}||_1||H^{\pi'}||_\infty && (\because \text{Hölder's inequality}) \\ &\quad\leq \frac{2\epsilon_R\gamma}{1-\gamma}\sqrt{D_{\mathrm{KL}}^{\max}(\mu||\pi')D_{\mathrm{KL}}^{\max}(\pi||\pi')} + \frac{\beta\gamma\epsilon_H}{1-\gamma}\sqrt{2D_{\mathrm{KL}}^{\max}(\pi||\pi')} && (\because \text{Lemma 4}) \\ &\quad= \frac{\gamma}{1-\gamma}\sqrt{D_{\mathrm{KL}}^{\max}(\pi||\pi')}\left(\sqrt{2}\beta\epsilon_H + 2\epsilon_R\sqrt{D_{\mathrm{KL}}^{\max}(\mu||\pi')}\right).\end{aligned}$$

If $\pi' = \pi$, the KL divergence term becomes zero, so equality holds. □

A.3 Proof of Theorem 2

We denote the policy parameter space as $\Psi \subseteq \mathbb{R}^d$, the parameter at the tth iteration as $\psi_t \in \Psi$, the Hessian matrix as $H(\psi_t) = \nabla_{\psi}^2 D_{\mathrm{KL}}(\pi_{\psi_t}||\pi_{\psi})|_{\psi=\psi_t}$, and the kth cost surrogate as $F_k(\psi_t) = F_k^{\mu,\pi}(\pi_{\psi_t};\alpha)$. As we focus on the tth iteration, the following notations are used for brevity: $H = H(\psi_t)$ and $g_k = \nabla F_k(\psi_t)$. The proposed gradient integration at tth iteration is defined as the following quadratic program (QP):

$$g_t = \mathop{\mathrm{argmin}}_{g} \frac{1}{2}g^T H g \quad \text{s.t. } g_k^T g + c_k \leq 0 \text{ for } \forall k, \tag{22}$$

where $c_k = \min(\sqrt{2\epsilon g_k^T H^{-1} g_k}, F_k(\pi_\psi;\alpha) - d_k + \zeta)$. In the remainder of this section, we introduce the assumptions and new definitions, discuss the existence of a solution (22), show the convergence to the feasibility condition for varying step size cases, and provide the proof of Theorem 2.

Assumption. **1)** Each F_k is differentiable and convex, **2)** ∇F_k is L-Lipschitz continuous, **3)** all eigenvalues of the Hessian matrix $H(\psi)$ are equal or greater than $R \in \mathbb{R}_{>0}$ for $\forall \psi \in \Psi$, and **4)** $\{\psi | F_k(\psi) + \zeta < d_k \text{ for } \forall k\} \neq \emptyset$.

Definition. Using the Cholesky decomposition, the Hessian matrix can be expressed as $H = B \cdot B^T$ where B is a lower triangular matrix. By introducing new terms, $\bar{g}_k := B^{-1} g_k$ and $b_t := B^T g_t$, the following is satisfied: $g_k^T H^{-1} g_k = ||\bar{g}_k||_2^2$. Additionally, we define the in-boundary and out-boundary sets as:

$$\text{IB}_k := \left\{ \psi | F_k(\psi) - d_k + \zeta \leq \sqrt{2\epsilon \nabla F_k(\psi)^T H^{-1}(\psi) \nabla F_k(\psi)} \right\},$$
$$\text{OB}_k := \left\{ \psi | F_k(\psi) - d_k + \zeta \geq \sqrt{2\epsilon \nabla F_k(\psi)^T H^{-1}(\psi) \nabla F_k(\psi)} \right\}.$$

The minimum of $||\bar{g}_k||$ in OB_k is denoted as m_k, and the maximum of $||\bar{g}_k||$ in IB_k is denoted as M_k. Also, $\min_k m_k$ and $\max_k M_k$ is denoted as m and M, respectively, and we can say that m is positive.

Lemma 5. *For all k, the minimum value of m_k is positive.*

Proof. Assume that there exist $k \in \{1, ..., K\}$ such that m_k is equal to zero at a policy parameter $\psi^* \in \text{OB}_k$, i.e., $||\nabla F_k(\psi^*)|| = 0$. Since F_k is convex, ψ^* is a minimum point of F_k, $\min_\psi F_k(\psi) = F_k(\psi^*) < d_k - \zeta$. However, $F_k(\psi^*) \geq d_k - \zeta$ as $\psi^* \in \text{OB}_k$, so m_k is positive due to the contradiction. Hence, the minimum of m_k is also positive. □

Lemma 6. *A solution of (22) always exists.*

Proof. There exists a policy parameter $\hat{\psi} \in \{\psi | F_k(\psi) + \zeta < d_k \text{ for } \forall k\}$ due to the assumptions. Let $g = \psi - \psi_t$. Then, the following inequality holds.

$$g_k^T(\psi - \psi_t) + c_k \leq g_k^T(\psi - \psi_t) + F_k(\psi_t) + \zeta - d_k \leq F_k(\psi) + \zeta - d_k. \quad (\because F_k \text{ is convex.})$$
$$\Rightarrow g_k^T(\hat{\psi} - \psi_t) + c_k \leq F_k(\hat{\psi}) + \zeta - d_k < 0 \text{ for } \forall k.$$

Since $\hat{\psi} - \psi_t$ satisfies all constraints of (22), the feasible set is non-empty and convex. Also, H is positive definite, so the QP has a unique solution. □

Lemma 6 shows the existence of solution of (22). Now, we show the convergence of the proposed gradient integration method in the case of varying step sizes.

Lemma 7. *If $\sqrt{2\epsilon}M \leq \zeta$ and a policy is updated by $\psi_{t+1} = \psi_t + \beta_t g_t$, where $0 < \beta_t < \frac{2\sqrt{2\epsilon}mR}{L||b_t||^2}$ and $\beta_t \leq 1$, the policy satisfies $F_k(\psi) \leq d_k$ for $\forall k$ within a finite time.*

Proof. We can reformulate the step size as $\beta = \frac{2\sqrt{2\epsilon}mR}{L||b_t||^2}\beta_t'$, where $\beta_t' \leq \frac{L||b_t||^2}{2\sqrt{2\epsilon}mR}$ and $0 < \beta_t' < 1$. Since the eigenvalues of H is equal to or bigger than R and H is symmetric and positive definite, $\frac{1}{R}I - H^{-1}$ is positive semi-definite. Hence, $x^T H^{-1} x \leq \frac{1}{R}||x||^2$ is satisfied. Using this fact, the following inequality holds:

$$\begin{aligned}
F_k(\psi_t + \beta_t g_t) - F_k(\psi_t) &\leq \beta_t \nabla F_k(\psi_t)^T g_t + \frac{L}{2}||\beta_t g_t||^2 \quad (\because \nabla F_k \text{ is } L\text{-Lipschitz continuous.}) \\
&= \beta_t g_k^T g_t + \frac{L}{2}\beta_t^2 ||g_t||^2 \\
&= \beta_t g_k^T g_t + \frac{L}{2}\beta_t^2 b_t^T H^{-1} b_t \qquad (\because g_t = B^{-T} b_t) \\
&\leq -\beta_t c_k + \frac{L}{2R}\beta_t^2 ||b_t||^2. \qquad (\because g_k^T g_t + c_k \leq 0)
\end{aligned}$$

Now, we will show that ψ enters IB_k in a finite time for $\forall\psi \in \mathrm{OB}_k$ and that the kth constraint is satisfied for $\forall\psi \in \mathrm{IB}_k$. Thus, we divide into two cases, **1)** $\psi_t \in \mathrm{OB}_k$ and **2)** $\psi_t \in \mathrm{IB}_k$. For the first case, $c_k = \sqrt{2\epsilon}||\bar{g}_k||$, so the following inequality holds:

$$\begin{aligned} F_k(\psi_t + \beta_t g_t) - F_k(\psi_t) &\leq \beta_t \left(-\sqrt{2\epsilon}||\bar{g}_k|| + \frac{L}{2R}\beta_t ||b_t||^2 \right) \\ &\leq \beta_t \sqrt{2\epsilon} \left(-||\bar{g}_k|| + m\beta'_t \right) \\ &\leq \beta_t \sqrt{2\epsilon} m(\beta'_t - 1) < 0. \end{aligned} \tag{23}$$

The value of F_k decreases strictly with each update step according to (23). Hence, ψ_t can reach IB_k by repeatedly updating the policy. We now check whether the constraint is satisfied for the second case. For the second case, the following inequality holds by applying $c_k = F_k(\psi_t) - d_k + \zeta$:

$$\begin{aligned} F_k(\psi_t + \beta_t g_t) - F_k(\psi_t) &\leq \beta_t d_k - \beta_t F_k(\psi_t) - \beta_t \zeta + \frac{L}{2R}\beta_t^2 ||b_t||^2 \\ \Rightarrow F_k(\psi_t + \beta_t g_t) - d_k &\leq (1 - \beta_t)(F_k(\psi_t) - d_k) + \beta_t(-\zeta + \sqrt{2\epsilon} m \beta'_t). \end{aligned}$$

Since $\psi_t \in \mathrm{IB}_k$,

$$F_k(\psi_t) - d_k \leq \sqrt{2\epsilon}||\bar{g}_k|| - \zeta \leq \sqrt{2\epsilon}M - \zeta \leq 0.$$

Since $m \leq M$ and $\beta'_t < 1$,

$$-\zeta + \sqrt{2\epsilon} m \beta'_t < -\zeta + \sqrt{2\epsilon}M \leq 0.$$

Hence, $F_k(\psi_t + \beta_t g_t) \leq d_k$, which means that the kth constraint is satisfied if $\psi_t \in \mathrm{IB}_k$. As ψ_t reaches IB_k for $\forall k$ within a finite time according to (23), the policy can satisfy all constraints within a finite time. □

Lemma 7 shows the convergence to the feasibility condition in the case of varying step sizes. We introduce a lemma, which shows $||b_t||$ is bounded by $\sqrt{\epsilon}$, and finally show the proof of Theorem 2, which can be considered a special case of varying step sizes.

Lemma 8. *There exists $T \in \mathbb{R}_{>0}$ such that $||b_t|| \leq T\sqrt{\epsilon}$.*

Proof. By solving the dual problem of (22), g_t can be expressed as:

$$g_t = -\sum_{k=1}^{K} \lambda_k H^{-1} g_k \text{ s.t. } \lambda_k = \max\left(\frac{c_k - \sum_{j \neq k} \lambda_j g_j^T H^{-1} g_k}{g_k^T H^{-1} g_k}, 0 \right) \text{ for } \forall k.$$

The following inequality holds for $\forall k$:

$$\lambda_k \leq \max\left(\frac{c_k}{||\bar{g}_k||^2}, 0 \right) \leq \max\left(\frac{\sqrt{2\epsilon}||\bar{g}_k||}{||\bar{g}_k||^2}, 0 \right) \leq \frac{\sqrt{2\epsilon}}{||\bar{g}_k||}.$$

Using triangular inequality,

$$\begin{aligned} ||b_t|| = ||B^T g_t|| = ||\sum_k \lambda_k B^T H^{-1} g_k|| &\leq \sum_k \lambda_k ||B^T H^{-1} g_k|| \\ &\leq \sqrt{2\epsilon} \sum_k \frac{||B^T H^{-1} g_k||}{||\bar{g}_k||} = K\sqrt{2\epsilon}. \end{aligned}$$

Hence, for every constant $T > \sqrt{2}K$, the statement holds. □

Theorem 2. *Assume that the cost surrogates are differentiable and convex, gradients of the surrogates are L-Lipschitz continuous, eigenvalues of the Hessian are equal or greater than a positive value $R \in \mathbb{R}_{>0}$, and $\{\psi | F_k(\pi_\psi; \alpha) + \zeta < d_k,\ \forall k\} \neq \emptyset$. Then, there exists $E \in \mathbb{R}_{>0}$ such that if $0 < \epsilon \leq E$ and a policy is updated by the proposed gradient integration method, all constraints are satisfied within finite time steps.*

Proof. The proposed step size is $\beta_t = \min(1, \sqrt{2\epsilon}/||b_t||)$, and the sufficient conditions that guarantee the convergence according to Lemma 7 are followings:

$$\sqrt{2\epsilon}M \leq \zeta \text{ and } 0 < \beta_t \leq 1 \text{ and } \beta_t < \frac{2\sqrt{2\epsilon}mR}{L||b_t||^2}.$$

The second condition is self-evident. To satisfy the third condition, the proposed step size β_t should satisfy the followings:

$$\frac{\sqrt{2\epsilon}}{||b_t||} < \frac{2\sqrt{2\epsilon}mR}{L||b_t||^2} \;\Leftrightarrow\; ||b_t|| < \frac{2mR}{L}.$$

If $\epsilon < 2((mR)/(LK))^2$, the following inequality holds:

$$\sqrt{2\epsilon} < \frac{2mR}{LK} \;\Rightarrow\; ||b_t|| \leq K\sqrt{2\epsilon} < \frac{2mR}{L}. \quad (\because \text{ Lemma 8.})$$

Hence, if $\epsilon \leq E = \frac{1}{2}\min(\frac{\zeta^2}{2M^2}, 2(\frac{mR}{LK})^2)$, the sufficient conditions are satisfied. □

A.4 Policy Update Rule

To solve the constrained optimization problem (13), we find a policy update direction by linearly approximating the objective and safety constraints and quadratically approximating the trust region constraint, as done by Achiam et al. (2017). After finding the direction, we update the policy using a line search method. Given the current policy parameter $\psi_t \in \Psi$, the approximated problem can be expressed as follows:

$$x^* = \underset{x \in \Psi}{\operatorname{argmax}}\; g^T x \quad \text{s.t. } \frac{1}{2}x^T H x \leq \epsilon,\; b_k^T x + c_k \leq 0\; \forall k, \tag{24}$$

where $g = \nabla_\psi J^{\mu,\pi}(\pi_\psi)|_{\psi=\psi_t}$, $H = \nabla_\psi^2 D_{\mathrm{KL}}(\pi_{\psi_t}||\pi_\psi)|_{\psi=\psi_t}$, $b_k = \nabla_\psi F_k^{\mu,\pi}(\pi_\psi;\alpha)|_{\psi=\psi_t}$, and $c_k = F_k(\pi_\psi;\alpha) - d_k$. Since (24) is convex, we can use an existing convex optimization solver. However, the search space, which is the policy parameter space Ψ, is excessively large, so we reduce the space by converting (24) to a dual problem as follows:

$$\begin{aligned} g(\lambda,\nu) &= \min_x L(x,\lambda,\nu) = \min_x\{g^T x + \nu(\frac{1}{2}x^T H x - \epsilon) + \lambda^T(Bx + c)\} \\ &= \frac{-1}{2\nu}\left(\underbrace{g^T H^{-1} g}_{=:q} + 2\underbrace{g^T H^{-1} B^T}_{=:r^T}\lambda + \lambda^T \underbrace{BH^{-1}B^T}_{=:S}\lambda\right) + \lambda^T c - \nu\epsilon \\ &= \frac{-1}{2\nu}(q + 2r^T\lambda + \lambda^T S\lambda) + \lambda^T c - \nu\epsilon, \end{aligned} \tag{25}$$

where $B = (b_1, .., b_K)$, $c = (c_1, ..., c_K)^T$, and $\lambda \in \mathbb{R}^K \geq 0$ and $\nu \in \mathbb{R} \geq 0$ are Lagrange multipliers. Then, the optimal λ and ν can be obtained by a convex optimization solver. After obtaining the optimal values, $(\lambda^*, \nu^*) = \operatorname{argmax}_{(\lambda,\nu)} g(\lambda,\nu)$, the policy update direction x^* are calculated by $\frac{-1}{\nu^*}H^{-1}(B^T\lambda^* + g)$. Then, the policy is updated by $\psi_{t+1} = \psi_t + \beta x^*$, where β is a step size, which can be calculated by a line search method.

B Ablation Study on Surrogate Functions

We have extended the off-policy TRPO (Meng et al., 2022) to the entropy-regularized version and reformulated it as the SAC-style version. In this section, we evaluate the original, entropy-regularized, and SAC-style versions in the continuous control tasks of the MuJoCo simulators (Todorov et al., 2012). We use neural networks with two hidden layers with (512, 512) nodes and ReLU for the activation function. The output of a value network is linear, but the input is different; the original and entropy-regularized versions use states, and the SAC-style version uses state-action pairs. The input of a policy network is the state, the output is mean μ and std σ, and actions are squashed into $\tanh(\mu + \epsilon\sigma)$, $\epsilon \sim \mathcal{N}(0,1)$ as in SAC (Haarnoja et al., 2018). The entropy coefficient β in the entropy-regularized and SAC-style versions are adaptively adjusted to keep the entropy above a

Parameter	
Discount factor γ	0.99
Trust region size ϵ	0.001
Length of replay buffer	10^5
Critic learning rate	0.0003
Trace-decay λ	0.97
Initial entropy coefficient β	1.0
β learning rate	0.01

Table 1: Hyperparameters for all versions.

threshold (set as $-d$ given $A \subseteq \mathbb{R}^d$). The hyperparameters for all versions are summarized in Table 1.

The training curves are presented in Figure 6. All methods are trained with five different random seeds. Since there is no importance ratio and the Q-functions directly provide policy update direction, the SAC-style version outperforms the others.

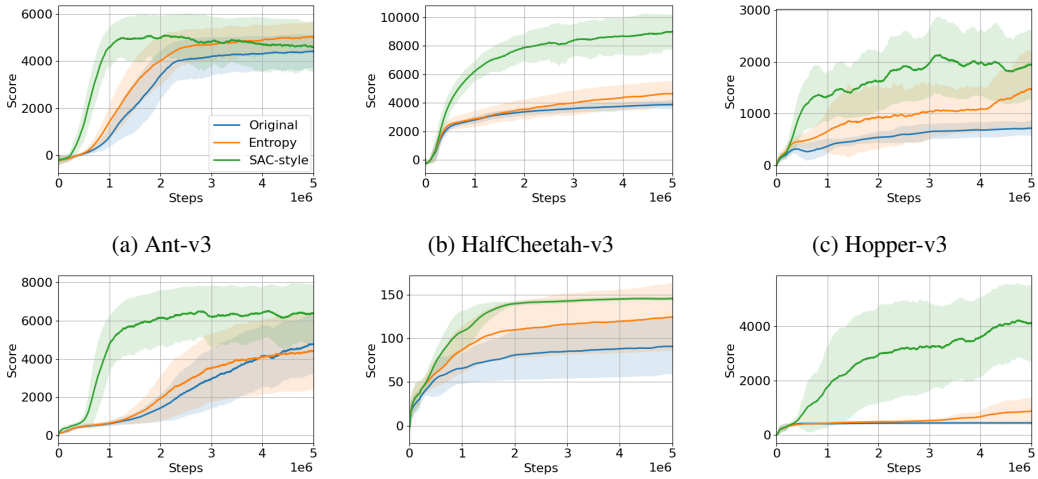

(a) Ant-v3 (b) HalfCheetah-v3 (c) Hopper-v3

(d) Humanoid-v3 (e) Swimmer-v3 (f) Walker2d-v3

Figure 6: MuJoCo training curves.

C Experimental Settings

Safety Gym. We use the goal and button tasks with the point and car robots in the Safety Gym environment (Ray et al., 2019), as shown in Figure 7a and 7b. The environmental setting for the goal task is the same as in Kim & Oh (2022b). Eight hazard regions and one goal are randomly spawned at the beginning of each episode, and a robot gets a reward and cost as follows:

$$\begin{aligned} R(s,a,s') &= -\Delta d_{\text{goal}} + \mathbf{1}_{d_{\text{goal}} \leq 0.3}, \\ C(s,a,s') &= \text{Sigmoid}(10 \cdot (0.2 - d_{\text{hazard}})), \end{aligned} \tag{26}$$

where d_{goal} is the distance to the goal, and d_{hazard} is the minimum distance to hazard regions. If d_{goal} is less than or equal to 0.3, a goal is respawned, and the number of constraint violations (CVs) is counted when d_{hazard} is less than 0.2. The state consists of relative goal position, goal distance, linear and angular velocities, acceleration, and LiDAR values. The action space is two-dimensional, which consists of xy-directional forces for the point and wheel velocities for the car robot.

The environmental settings for the button task are the same as in Liu et al. (2022). There are five hazard regions, four dynamic obstacles, and four buttons, and all components are fixed throughout the training. The initial position of a robot and an activated button are randomly placed at the

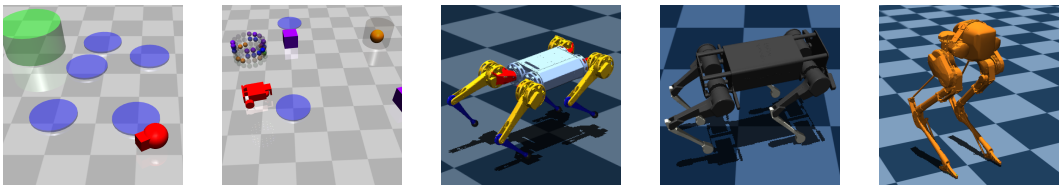

(a) Point goal. (b) Car button. (c) Mini-Cheetah. (d) Laikago. (e) Cassie.

Figure 7: (a) and (b) are Safety Gym tasks. (c), (d), and (e) are locomotion tasks.

beginning of each episode. The reward function is the same as in (26), but the cost is different since there is no dense signal for contacts. We define the cost function for the button task as an indicator function that outputs one if the robot makes contact with an obstacle or an inactive button or enters a hazardous region. We add LiDAR values of buttons and obstacles to the state of the goal task, and actions are the same as the goal task. The length of the episode is 1000 steps without early termination.

Locomotion Tasks. We use three different legged robots, Mini-Cheetah, Laikago, and Cassie, for the locomotion tasks, as shown in Figure 7c, 7d, and 7e. The tasks aim to control robots to follow a velocity command on flat terrain. A velocity command is given by $(v_x^{\text{cmd}}, v_y^{\text{cmd}}, \omega_z^{\text{cmd}})$, where $v_x^{\text{cmd}} \sim \mathcal{U}(-1.0, 1.0)$ for Cassie and $\mathcal{U}(-1.0, 2.0)$ otherwise, $v_y^{\text{cmd}} = 0$, and $\omega_z^{\text{cmd}} \sim \mathcal{U}(-0.5, 0.5)$. To lower the task complexity, we set the y-directional linear velocity to zero but can scale to any non-zero value. As in other locomotion studies (Lee et al., 2020; Miki et al., 2022), *central phases* are introduced to produce periodic motion, which are defined as $\phi_i(t) = \phi_{i,0} + f \cdot t$ for $\forall i \in \{1, ..., n_{\text{legs}}\}$, where f is a frequency coefficient and is set to 10, and $\phi_{i,0}$ is an initial phase. Actuators of robots are controlled by PD control towards target positions given by actions. The state consists of velocity command, orientation of the robot frame, linear and angular velocities of the robot, positions and speeds of the actuators, central phases, history of positions and speeds of the actuators (past two steps), and history of actions (past two steps). A foot contact timing ξ can be defined as follows:

$$\xi_i(s) = -1 + 2 \cdot \mathbf{1}_{\sin(\phi_i) \leq 0} \quad \forall i \in \{1, ..., n_{\text{legs}}\}, \tag{27}$$

where a value of -1 means that the ith foot is on the ground; otherwise, the foot is in the air. For the quadrupedal robots, Mini-Cheetah and Laikago, we use the initial phases as $\phi_0 = \{0, \pi, \pi, 0\}$, which generates trot gaits. For the bipedal robot, Cassie, the initial phases are defined as $\phi_0 = \{0, \pi\}$, which generates walk gaits. Then, the reward and cost functions are defined as follows:

$$\begin{gathered} R(s, a, s') = -0.1 \cdot (||v_{x,y}^{\text{base}} - v_{x,y}^{\text{cmd}}||_2^2 + ||\omega_z^{\text{base}} - \omega_z^{\text{cmd}}||_2^2 + 10^{-3} \cdot R_{\text{power}}), \\ C_1(s, a, s') = \mathbf{1}_{\text{angle} \geq a}, \; C_2(s, a, s') = \mathbf{1}_{\text{height} \leq b}, \; C_3(s, a, s') = \sum_{i=1}^{n_{\text{legs}}} (1 - \xi_i \cdot \hat{\xi}_i)/(2 \cdot n_{\text{legs}}), \end{gathered} \tag{28}$$

where the power consumption $R_{\text{power}} = \sum_i |\tau_i v_i|$, the sum of the torque times the actuator speed, is added to the reward as a regularization term, $v_{x,y}^{\text{base}}$ is the xy-directional linear velocity of the base frame of robots, ω_z^{base} is the z-directional angular velocity of the base frame, and $\hat{\xi} \in \{-1, 1\}^{n_{\text{legs}}}$ is the current feet contact vector. For balancing, the first cost indicates whether the angle between the z-axis vector of the robot base and the world is greater than a threshold ($a = 15°$ for all robots). For standing, the second cost indicates the height of CoM is less than a threshold ($b = 0.3, 0.35, 0.7$ for Mini-Cheetah, Laikago, and Cassie, respectively), and the last cost is to check that the current feet contact vector $\hat{\xi}$ matches the pre-defined timing ξ. The length of the episode is 500 steps. There is no early termination, but if a robot falls to the ground, the state is frozen until the end of the episode.

Hyperparameter Settings. The structure of neural networks consists of two hidden layers with $(512, 512)$ nodes and ReLU activation for all baselines and the proposed method. The input of value networks is state-action pairs, and the output is the positions of atoms. The input of policy networks is the state, the output is mean μ and std σ, and actions are squashed into $\tanh(\mu + \epsilon\sigma)$, $\epsilon \sim \mathcal{N}(0, 1)$. We use a fixed entropy coefficient β. The trust region size ϵ is set to 0.001 for all trust region-based methods. The overall hyperparameters for the proposed method can be summarized in Table 2. Since the range of the cost is $[0, 1]$, the maximum discounted cost sum is $1/(1 - \gamma)$. Thus,

Parameter	Safety Gym	Locomotion
Discount factor γ	0.99	0.99
Trust region size ϵ	0.001	0.001
Length of replay buffer	10^5	10^5
Critic learning rate	0.0003	0.0003
Trace-decay λ	0.97	0.97
Entropy coefficient β	0.0	0.001
The number of critic atoms M	25	25
The number of target atoms M'	50	50
Constraint conservativeness α	0.5 and 1.0	1.0
Limit value d_k	$0.025/(1-\gamma)$	$[0.025, 0.025, 0.4]/(1-\gamma)$
Slack coefficient ζ	-	$\min_k d_k = 0.025/(1-\gamma)$
Reward shaping weights w_i	-	$[5.19, 3.71, 0.34]$

Table 2: Hyperparameter settings for the Safety Gym and locomotion tasks.

the limit value is set by target cost rate times $1/(1-\gamma)$. For the locomotion tasks, the third cost in (28) is designed for foot stamping, which is not essential to safety. Hence, we set the limit value to near the maximum (if a robot does not stamp, the cost rate becomes 0.5). The reward shaping weights are also presented in Table 2, which are optimized using the existing Bayesian optimization tool. In addition, baseline methods use multiple critic networks for the cost function, such as target (Yang et al., 2021) or square value networks (Kim & Oh, 2022a). To match the number of network parameters, we use two critics as an ensemble, as in Kuznetsov et al. (2020).

D Experimental Results

D.1 Safety Gym

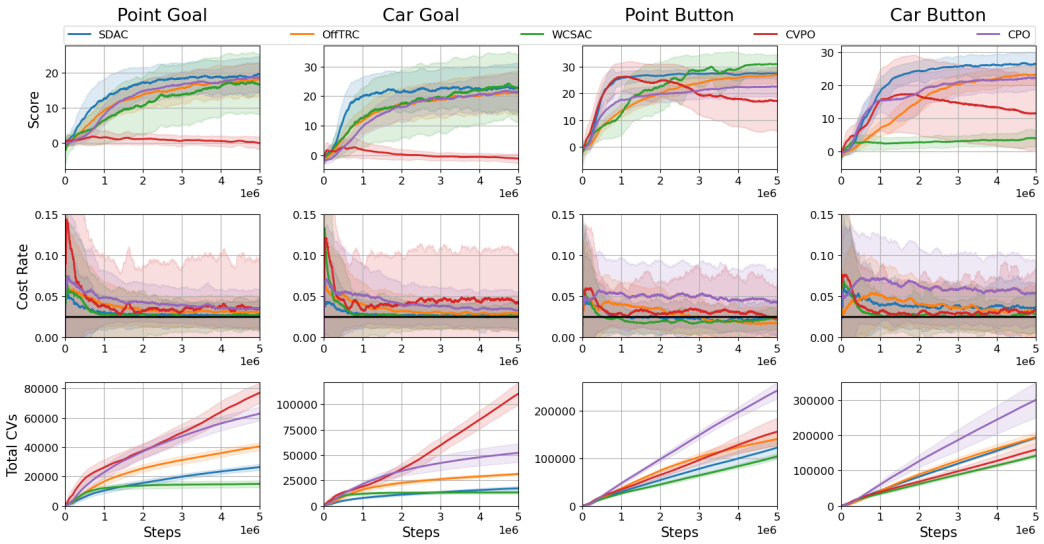

Figure 8: Training curves of mean constrained algorithms for the Safety Gym tasks. The solid line and shaded area represent the average and std values, respectively. The solid black lines in the second row indicate limit values. All methods are trained with five random seeds.

In this section, we present the training curves of the Safety Gym tasks separately according to the conservativeness of constraints for better readability. Figure 8 shows the training results of the mean constrained and mean-std constrained algorithms with $\alpha = 1.0$. Figures 9 and 10 show the training results of the mean-std constrained algorithms with $\alpha = 0.25$ and 0.5, respectively. In Figure 8, it can be observed that the score of SDAC has the fastest convergence speed and that the cost rates

also converge to the limit values quickly. Observing that all the other methods show the highest total CVs in the car button task, this task is challenging to meet the constraint. Thus, SDAC also has a higher cost rate for the car button than other tasks. In addition, since decreasing α makes the constraints more conservative, the cost rates and the number of total CVs of SDAC are reduced in Figures 9 and 10. For $\alpha = 0.25$ and 0.5, SDAC shows the highest scores and the lowest number of CVs in all tasks.

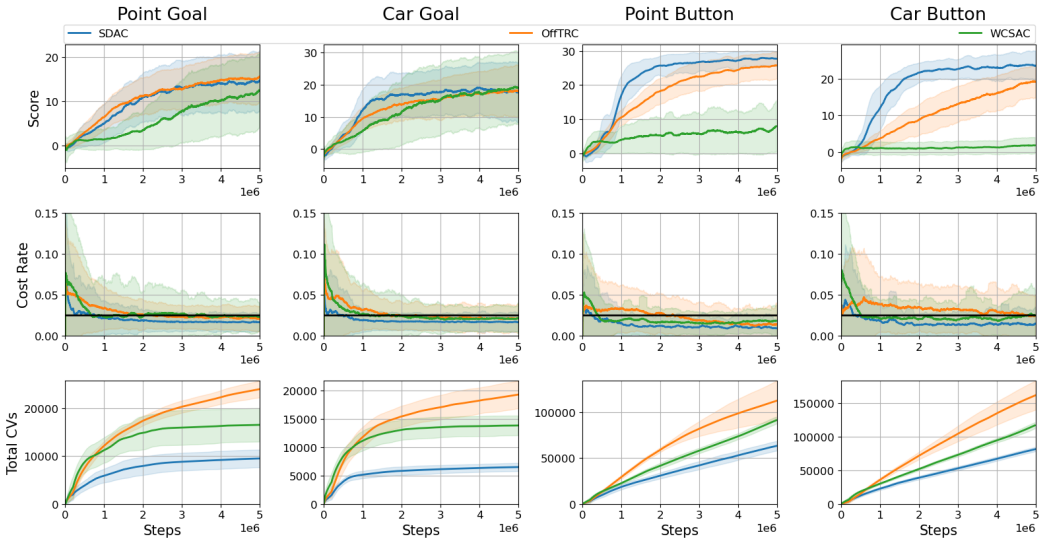

Figure 9: Training curves of mean-std constrained algorithms with $\alpha = 0.5$ for the Safety Gym.

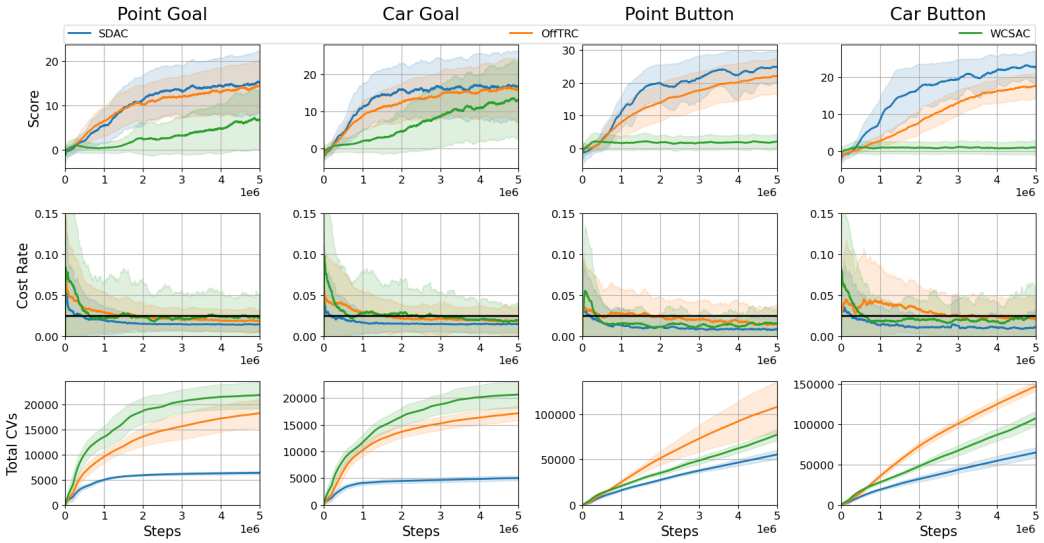

Figure 10: Training curves of mean-std constrained algorithms with $\alpha = 0.25$ for the Safety Gym.

D.2 LOCOMOTION TASKS

We present the training curve for the locomotion tasks in Figure 11, where the true reward is defined in (28). The traditional RL baselines are trained with the reward $\bar{R} = (R - \sum_{i=1}^{3} w_i C_i)/(1 + \sum_{i=1}^{3} w_i)$, and the weights are described in Section C. The training curve contains graphs of the three cost rates and the true reward sum.

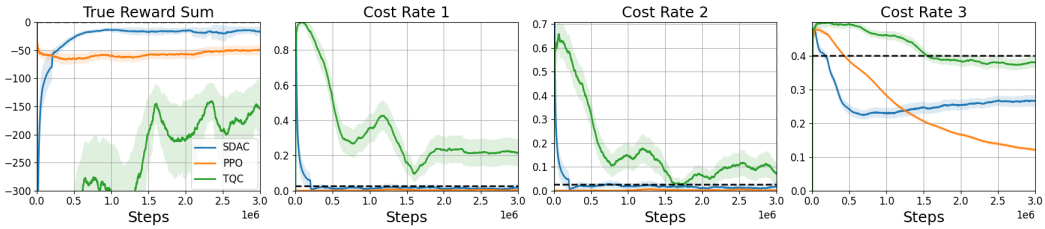

(a) Mini-Cheetah.

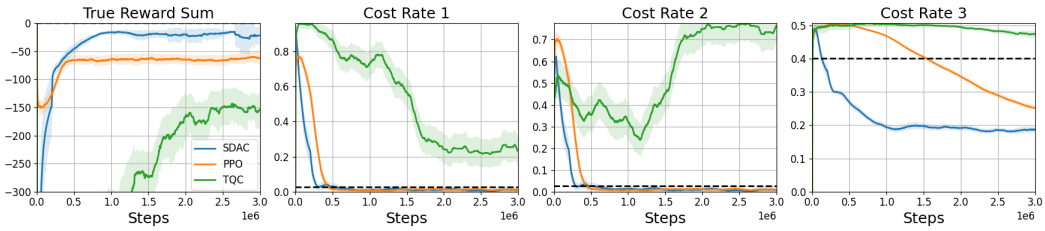

(b) Laikago.

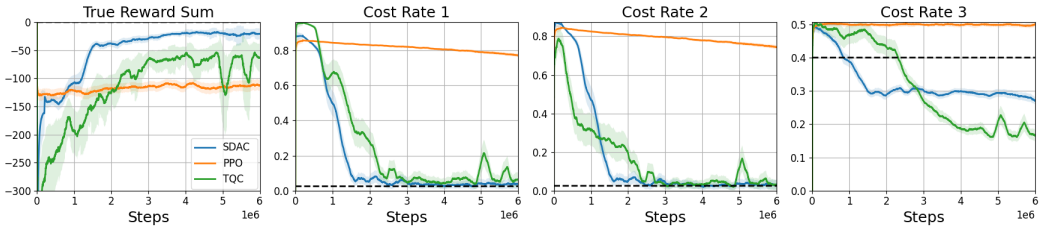

(c) Cassie.

Figure 11: Training curves of the locomotion tasks. The black dashed lines show the limit values used for the safe RL methods. The solid line represents the average value, and the shaded area shows one-fifth of the std value. All methods are trained with five different random seeds.

D.3 Ablation Study on Components of SDAC

We experiment with variations of SDAC to examine the effectiveness of each component. SDAC has two main components, SAC-style surrogate functions and distributional critics. We call SDAC with only distribution critics, *SDAC-Dist*, and SDAC with only SAC-style surrogates, *SDAC-Q*. If all components are absent, SDAC is identical to OffTRC (Kim & Oh, 2022a). The variants are trained with the point goal task of the Safety Gym, and the training results are shown in Figure 12. SDAC-Q lowers the cost rate quickly but shows the lowest score. SDAC-Dist shows scores similar to SDAC, but the cost rate converges above the limit value 0.025. In conclusion, SDAC can efficiently satisfy the safety constraints through the SAC-style surrogates and improve score performance through the distributional critics.

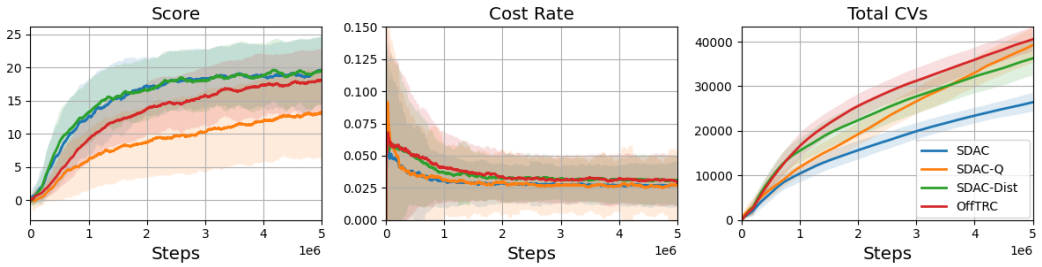

Figure 12: Training curves of variants of SDAC for the point goal task.

D.4 Ablation Study on Hyperparameters

To check the effects of the hyperparameters, we conduct ablation studies on the trust region size and entropy coefficient. The results are shown in Figure 13. From the entropy coefficient results, it can be seen that excessive exploration causes the constraint to be violated. Thus, the entropy coefficient should be adjusted cautiously, or it can be better to set the coefficient to zero. Since Theorem 1 shows that the estimation error of the surrogates is proportional to the trust region size, it can be observed from Figure 13b that the number of CVs increases with the size of the trust region due to the estimation error.

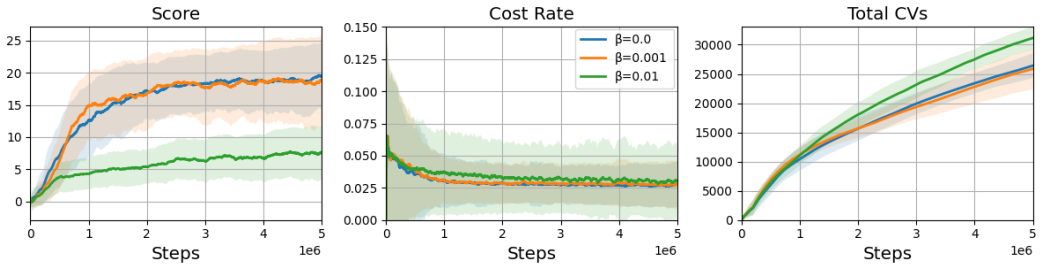

(a) Entropy coefficient β.

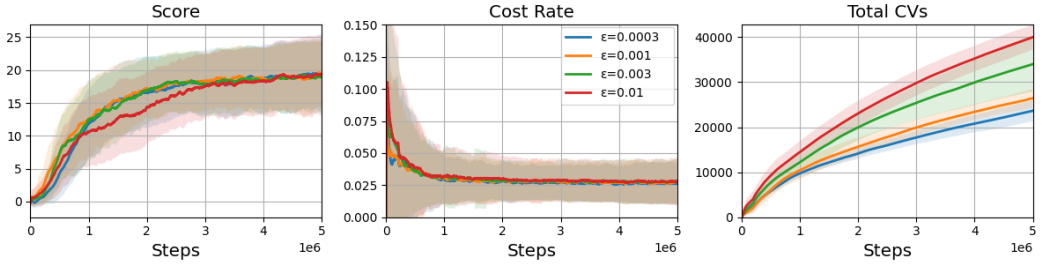

(b) Trust region size ϵ.

Figure 13: Training curves of SDAC with different hyperparameters for the point goal task.